UNIWERSYTET WARSZAWSKI

MIĘDZYWYDZIAŁOWE INDYWIDUALNE STUDIA MATEMATYCZNO–PRZYRODNICZE

Grzegorz Brona
186526

Search for pentaquark states in the COMPASS experiment

Praca magisterska
W Zakładzie Cząstek i Oddziaływań Fundamentalnych
Wydziału Fizyki
Pod kierunkiem prof. Barbary Badełek

WARSZAWA, 2004

The most beautiful thing we can experience is the mysterious. It is the source of all true art and science.

Albert Einstein

Abstract

The thesis describes a search for the Θ^+ and $\Xi_{3/2}$ pentaquark states in the COMPASS data taken in 2002. In case of Θ^+ its decay channel $\Theta^+ \to pK^0 \to p\pi^+\pi^-$ is studied. The $\Xi_{3/2}$ pentaquark is predicted to exists in four charge states: $\Xi^{--}_{3/2}$, $\Xi^{0}_{3/2}$, $\Xi^{-}_{3/2}$, $\Xi^{+}_{3/2}$. Studies of $\Xi^{--}_{3/2}$ and $\Xi^{0}_{3/2}$ are performed. The search is focused on $\Xi^{--}_{3/2} \to \Xi^-\pi^- \to \Lambda^0\pi^-\pi^- \to p\pi^-\pi^-\pi^-$ and $\Xi^{0}_{3/2} \to \Xi^-\pi^+ \to \Lambda^0\pi^-\pi^+ \to p\pi^-\pi^-\pi^+$ decay channels. The studies of the antipentaquarks decay channels are also performed. The K^0, Λ^0, $\overline{\Lambda^0}$, Ξ^-, $\overline{\Xi^-}$ particles are reconstructed and cuts leading to their most efficient selection are investigated. A comparison between yields of K^0 and Λ^0 predicted by Monte Carlo and found in Real Data is done. Studies of $\Lambda^0(1520)$ and $\Xi^0(1530)$ are also performed since the decay channels of these particles are similar to those of the pentaquarks. Upper limit for the $\Xi_{3/2}$ pentaquark states production in the μN interactions in COMPASS is given.

Contents

List of Figures

List of Tables

Chapter 1

Introduction

1.1 The quark model

Quarks and gluons are considered to be fundamental building blocks of matter at the scales presently achieved in the experiments. The first Static Quark Model was proposed in 1964 by Gell-Mann and Zweig in order to explain symmetries observed in the hadron spectroscopy. The model was based on an assumption that all known hadrons were composed of three different quarks. The quarks were named: up (u), down (d) and strange (s). All known hadrons were grouped into two families: mesons and baryons. Mesons were composed of a valence quark and antiquark ($q\overline{q}$) while baryons contained three valence quarks (qqq). In the early seventies theorists added a fourth quark – charm (c) – to the Static Quark Model. In 1974 a J/ψ meson, the first particle which contained charmed quarks, was observed. This was a striking evidence for the correctness of the model. Later two more quarks were discovered – bottom (b) and top (t). With the discovery of gluons and the development of a field theory for the strong interactions – Quantum ChromoDynamics (QCD) – a dynamical picture of hadrons was created. Presently the QCD improved quark model, encompassing static as well as dynamic description of hadrons, is well established and gives a wide range of predictions about the existence of new hadron states. According to the model, ground state baryons composed of three valence quarks: u, d or s form two multiplets – an octet with quantum numbers $J^P = 1/2^+$ and a decuplet with $J^P = 3/2^+$. Within this model a spectrum of other three-quark baryons (containing u, d or s valence quarks) of different masses may exist as excited states of particles from these two multiplets.

1.2 Pentaquark states

The existence of baryons containing more than three valence quarks is not forbidden by the quark model. Some of these states would have the quantum numbers identical to those for three-quarks baryons and therefore they would decay in the same channels as three-quarks states. Others, which are called exotic ones, would have quantum numbers which cannot be constructed from three quarks only and thus their misidentification as three-quarks baryons would be impossible.

A pentaquark is a particle containing five valence quarks ($qqqq\overline{q}$). In the seventies and eighties, several experiments were looking for pentaquarks. Two possible candidates were found – $Z_0(1780)$ and $Z_0(1865)$. However in both cases the evidence for their existence was very poor. In 1986 the Particle Data Group (PDG) mentioned possible exotic resonances in the baryon listing [1].

In 1987 a prediction on pentaquark masses was made by Praszałowicz [2]. It was based on a chiral soliton model of the nucleon. Praszałowicz and later Diakonov, Petrov and Polyakov [3] found that one of the consequences of this model is the existence of an antidecuplet of 10 ground-state pentaquarks, three of which are exotic. Assuming that one of the particles entering the antidecuplet is a known $N(1710)P_{11}$ non–exotic state, it is possible to deduce the mass of the lightest state of this multiplet. This state is called Θ^+, it is exotic, and according to predictions its mass is about 1530 MeV and width smaller than 15 MeV. The valence quarks configuration of the Θ^+ state is $uudd\overline{s}$. The particle decays in two channels:

$$\Theta^+ \to pK^0 \tag{1.1}$$

$$\Theta^+ \to nK^+ \tag{1.2}$$

Several experiments have recently announced an observation of a narrow state of mass around 1530 MeV which probably corresponds to the Θ^+ pentaquark. The experiments are: SPring-8 (LEPS) [4], CLAS (JLAB) [5,6], DIANA (ITEP) [7], SAPHIR (ELSA) [8], HERMES (DESY) [9], ZEUS (DESY) [10], SVD-2 (ITEP) [11] and bubble chamber neutrino experiments [12].

An observation of another two states corresponding to heavier pentaquark multiplet members has been reported by NA49 (CERN) [13]. These states contain two strange quarks and are called $\Xi^{--}_{3/2}$ ($ddss\overline{u}$) and $\Xi^{0}_{3/2}$ ($udss\overline{d}$).

Recently the H1 collaboration (DESY) [14] announced an observation of a pentaquark containing one charmed quark ($uudd\overline{c}$).

1.2.1 Observations of the Θ^+ state

The signal of the Θ^+ pentaquark has been observed in both nK^+ and pK^0 decay channels. Experiments that reported the observation used various beams, various targets and covered a wide spectrum of the center-of-mass energy. Several of them selected a Θ^+ formation regime and others a production regime. Characteristics of the experiments are listed in Table 1.1.

Experiment	Beam	Target	Beam energy [GeV]	Studied decay channel
SPring-8	γ	H + C	<2.4	nK^+
CLAS	γ	H ; D	<5.5	nK^+
SAPHIR	γ	H	<2.6	nK^+
DIANA	K^+	Xe	<0.85	pK^0
HERMES	e^+	D	27.5	pK^0
SVD-2	p	C, Si, Pb	70.0	pK^0
Bubble chambers	ν, $\overline{\nu}$	H, D, Ne	40÷140	pK^0
ZEUS	$e^+ - p$	—	27.5+820;27.5+920	pK^0

Table 1.1: Characteristics of experiments that reported an observation of the Θ^+ pentaquark state.

Each of the experiments found a narrow peak located at the mass range between 1520 and 1560 MeV with a FWHM smaller than 25 MeV (the FWHM was in each experiment consistent with its instrumental resolution). Characteristics of the Θ^+ peaks are presented in Table 1.2. Two different methods were used to estimate the significance of these peaks: $S/\sqrt{B}$ (DIANA, CLASS, SPring-8, HERMES, SVD-2) and $S/\sqrt{B+S}$ (SAPHIR, HERMES). Here S and B stand for signal and background respectively.

Of the above mentioned experiments, HERMES is the most similar to COMPASS. It uses a 27.5 GeV positron beam from the HERA storage ring and a stationery target. The studied reaction is a quasi-real photoproduction on the deuteron. Data used in the analysis have an integrated luminosity of 250 pb^{-1}. Identification of pions and protons is achieved by the RICH detector. A cross contamination of pions and protons is negligible if the samples are restricted to momentum ranges 1–15 GeV for pions and 4–9 GeV for protons (for comparison, the momentum thresholds for pions and protons identification in COMPASS are about 2.5 GeV and about 17 GeV respectively, see Sec. 2).

Experiment	Θ^+ mass [MeV]	FWHM [MeV]	Significance
SPring-8	$1540 \pm 10 \pm 5$	25	4.6
CLAS(d)	$1542 \pm 2 \pm 5$	21	5.2
CLAS(p)	$1555 \pm 1 \pm 10$	26 ± 7	7.8
DIANA	$1539 \pm 2 \pm few$	9	4.4
SAPHIR	$1540 \pm 4 \pm 2$	25	4.8
HERMES	$1528 \pm 2.6 \pm 2.1$	$19 \pm 5 \pm 2$	4–6
SVD-2	$1526 \pm 3 \pm 3$	24	5.6
Bubble chambers	1533 ± 5	20	6.7
ZEUS	$1521.5 \pm 1.5 \pm 2.8$	15	3.9–4.6

Table 1.2: Summary of Θ^+ signals in different experiments (extended version of Table III in [9]).

1.2.2 Observation of $\Xi_{3/2}$ states

Pentaquark states that contain two strange quarks should have masses in the range of 1700–2100 MeV and widths a few times larger than the width of Θ^+ [3], [15]. There should exist four such states forming an isospin quartet ($\Xi^{--}_{3/2}$, $\Xi^{-}_{3/2}$, $\Xi^{0}_{3/2}$, $\Xi^{+}_{3/2}$). A possible observation of two of them was reported by the NA49 experiment at CERN [13]. The experiment uses a 158 GeV proton beam. The incident protons interact with a liquid hydrogen target. The target is 20 cm long and 2 cm in diameter. Tracks of the charged final state particles are reconstructed in the time projection chambers (TPC). The identification of the particles is performed also in TPCs by measuring the energy loss (dE/dx). The COMPASS detector works at the same beam energy but the reactions studied are muon–nucleon rather than nucleon–nucleon. NA49 found a pentaquark signal in three channels, in each at the mass of about 1862 MeV:

$$\Xi^{--}_{3/2} \to \Xi^{-}\pi^{-} \to \Lambda^0\pi^-\pi^- \to p\pi^-\pi^-\pi^- \tag{1.3}$$

$$\Xi^{0}_{3/2} \to \Xi^{-}\pi^{+} \to \Lambda^0\pi^-\pi^+ \to p\pi^-\pi^-\pi^+ \tag{1.4}$$

$$\overline{\Xi^{--}_{3/2}} \to \overline{\Xi^{-}}\pi^{+} \to \overline{\Lambda^0}\pi^+\pi^+ \to \overline{p}\pi^+\pi^+\pi^+ \tag{1.5}$$

but the signal was absent in the channel:

$$\overline{\Xi^{0}_{3/2}} \to \overline{\Xi^{-}}\pi^{-} \to \overline{\Lambda^0}\pi^+\pi^- \to \overline{p}\pi^+\pi^+\pi^- \tag{1.6}$$

After summing up events from all four channels the signal had statistical significance of 5.6 σ and the width of 17 MeV. The significance was calculated as $S/\sqrt{B+S}$.

In connection with the NA49 observation, a critical analysis of previous experiments investigating $\Xi\pi$ invariant mass distribution was performed [16]. Only experiments of statistics comparable or greater than NA49 were examined. None of them reported a peak in the mass region around 1860 MeV.

1.2.3 Observation of a charmed pentaquark

Recently the H1 collaboration has announced an observation of a narrow resonance present in both $D^{*+}\overline{p}$ and $D^{*-}p$ invariant mass distributions [14]. The resonance has a mass (3099 $\pm$ 3 $\pm$ 5) MeV and a width of (12 $\pm$ 3) MeV. Statistical significance of a combined signal is 5.4 σ. The resonance is interpreted as a charmed pentaquark – $(uudd\overline{c})$.

1.2.4 Search for pentaquark states in the COMPASS experiment

In the COMPASS experiment it is possible to search for the Θ^+ and $\Xi_{3/2}$ pentaquarks in the decay channels in which only charged particles are produced. In this thesis a description of the search for both pentaquark states is presented. The analysis was performed on the data taken in 2002 since the data from 2003 were not available yet. The center-of-mass energy in the COMPASS experiment is too low to study the charmed pentaquark state observed by H1.

Chapter 2

The COMPASS detector

COMPASS (code NA58) is a high-energy experiment at CERN. Its physics programme is two-fold: a spin physics with a polarized muon beam and a polarized target and a hadron physics with hadronic beams and nuclear targets. The muon programme started in 2002 and will last until 2004. The hadron programme will begin after 2005. The analysis performed in this thesis covers data taken in 2002, *i.e.* during the first year of the muon programme. In this chapter a short description of the detector setup used during the data taking is given.

2.1 Beam

The COMPASS detector is located at the Super Proton Synchrotron (SPS) at CERN. A 400 GeV proton beam from SPS interacts with a beryllium target placed about one kilometer upstream the COMPASS experimental hall. The interactions result in a beam of secondary particles: p^+, K^+, π^+, K^-, and π^-. About 400 meters upstream the hall a heavy absorber is placed on the secondary beam trajectory. Before reaching the absorber almost all the pions decay into muons and muon neutrinos. The remaining hadrons are stopped inside the absorber while the muons pass through loosing only a small fraction of their initial energy. Downstream the absorber a set of magnets is located. Their task is to form a muon beam. In 2002 a positive 160 GeV muon beam of intensity about $2 \cdot 10^8 \mu$/spill was used in the experiment. Each spill lasted about 4.8 s. The beam was naturally polarized. The neutrinos are left-handed particles, which means that their spin and momentum vectors are antiparallel. Therefore muons from the $\pi^+ \to \mu^+\nu$ decays are also left-handed in the pion center-of-mass (CM) frame. In the laboratory system this corresponds to the 160 GeV muon beam polarization of 76%.

2.2 Target

In order to measure spin dependent interactions a polarized target is used in COMPASS. The target – two cells 60 cm long and 3 cm in a diameter – is filled with a solid lithium deuteride, ^{6}LiD. The cells are located inside a superconducting solenoid which provides a magnetic field of 2.5 T. The target is cooled down to a temperature of 50 mK by ^{3}He–^{4}He refrigerator. Target cells are polarized up to about 50% in opposite directions using the dynamic nuclear polarization method. The polarization is reversed every 8 hours. The target material is not pure. Apart from the lithium deuteride it contains a nonnegligible contamination of other elements. Composition of the target material is given in Table 2.1.

Element	No. of mols	Atomic mass	Element	No. of mols	Atomic mass
H	0.1019	1	^{7}Li	1.7950	7
D	44.5370	2	C	0.0080	12
^{3}He	3.6207	3	F	0.0160	19
^{4}He	10.9118	4	Ni	0.0057	58.6
^{6}Li	42.8429	6	Cu	0.0136	63.6

Table 2.1: Composition of the target material.

2.3 Spectrometer

The COMPASS detector is composed of two separate spectrometers. The Large Angle Spectrometer (LAS) is designed to detect and identify particles with emission angles greater than 30 mrad with respect to the beam direction. The second spectrometer – Small Angle Spectrometer (SAS) – is optimized for measuring particles with emission angles smaller than 30 mrad. Such a two stage-spectrometer allows an efficient detection of both slow and fast particles leaving the interaction point located inside the COMPASS target. Both spectrometers are composed in a similar way. To measure particles momenta the spectrometers are equipped with magnets (SM1 of 1 Tm in LAS, SM2 of 5 Tm in SAS). Tracks of particles that go through a magnetic field are deflected. By measuring this deflection with tracking stations located in front of and behind the magnets, values of particle momenta are obtained. Identification of particles with known momenta is performed in a Ring Imaging CHerenkov counter, RICH. In 2002 only RICH1, which is a part of the LAS

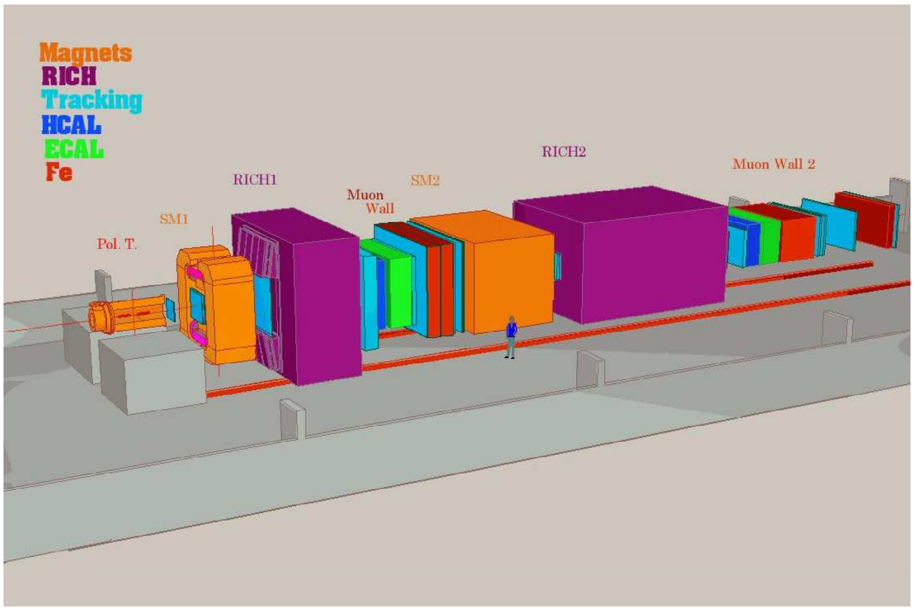

Figure 2.1: The COMPASS spectrometer.

detector, was operating. A second RICH will probably be added during the hadron programme after 2005. RICH1 is able to separate pions, kaons and protons in a wide range of momenta from a few GeV up to about 50 GeV. Pions can be identified if their momenta exceed about 2.5 GeV. Kaons can be identified from about 9 GeV. For protons identification momenta higher than 17 GeV are required. Several different kinds of tracking detectors are used in both stages of the COMPASS spectrometer. Scintillation Fibers (SciFi) and Silicon Microstrips (SI) are used for tracking at a very small angles with respect to the beam direction. These detectors can work efficiently with high particle intensity and thus close to the beam region. Further away from the beam the Gas Electron Multipliers (GEM) are located. The large angle tracking is performed by the Drift Chambers (DC), Straw Tubes (ST) and Micro Mesh gas detectors (Micromegas). Both spectrometers contain hadronic calorimeters (HCAL1 and HCAL2). Their task is to measure the energy of the through-going hadrons. The electromagnetic calorimeters (ECAL1 and ECAL2) were not used in the 2002 data taking. Two "muon walls" or "muon filters" (μF1 and μF2) perform the muon identification. Muons are the only particles that are able to pass the muon walls and give signals in tracking detectors downstream the walls. A few additional detectors will be added for the hadron programme. However also the muon programme setup of the COMPASS experiment can be used for hadron spectroscopy, as it will be shown in this work.

Chapter 3

Methods and tools

In this chapter methods and tools used in the pentaquark analysis in COMPASS are described. First the pentaquark decay channels are discussed. Then Armenteros variables, which are useful in the studies of secondary vertices, are presented. Finally the data set and the used computer software are described.

3.1 Pentaquark decay channels

Two different pentaquark states are searched for in this paper: the Θ^+ and the $\Xi_{3/2}$. Both states decay *via* strong interactions and thus their decay vertices are located very close to the interaction points in which the states were produced. Therefore after the reconstruction, particles originating from the pentaquark decays are ascribed to primary vertices. Studies of the primary interaction points and their characteristics are described in Sec. 4.

The Θ^+ pentaquark state containing one $\overline{s}$ quark decays into a pK^0 pair. The K^0 and $\overline{K^0}$ particles are eigenstates of the strong and electromagnetic interactions. However strangeness is not conserved in the weak interactions and therefore, in this kind of interactions, K^0 and $\overline{K^0}$ can not be distinguished. Thus in the weak K^0 or $\overline{K^0}$ decays one can only make a distinction between two independent linear combinations of those states. The combinations differ by their CP value. A state with $CP = 1$ is called K^0_S or K_{short} and a state with $CP = -1$ is called K^0_L or K_{long}, due to their average lifetimes which are $\tau_S = (0.8937 \pm 0.0012) \cdot 10^{-10}$ s and $\tau_L = (5.17 \pm 0.04) \cdot 10^{-8}$ s, respectively. In the COMPASS spectrometer only K^0_S particles can be detected since K^0_L lifetime is too long for these particles to decay inside the detector. The K^0_S particles decay into two oppositely charged pions: $K^0_S \to \pi^+\pi^-$ (68.60%) and into: $K^0_S \to \pi^0\pi^0$ (31.40%). Two neutral π^0 mesons in the final state cannot be reconstructed with the

2002 COMPASS setup. Similarly the Θ^+ decay into nK^+ cannot be detected since the neutron escapes undetectable from the detector. The first step in the Θ^+ search is focused on K^0_S reconstruction. This employs reconstruction of secondary vertices (Sec. 5.1). Then the K^0_S particles are combined with protons from primary vertices (Sec. 7). In what follows K^0_S particle will be denoted as K^0.

The pentaquark $\Xi_{3/2}$ particles form a family consisting of four different states, each containing two s quarks. Two of these states can be studied with the COMPASS detector: $\Xi^0_{3/2}$ and $\Xi^{--}_{3/2}$. Pentaquark $\Xi^0_{3/2}$ decays into Ξ^- and π^+, while the $\Xi^{--}_{3/2}$ decays into Ξ^- and π^-. The other two states, $\Xi^+_{3/2}$ and $\Xi^-_{3/2}$, contain neutral π^0 mesons among the decay products and thus cannot be detected with the 2002 spectrometer setup. The lifetime of the Ξ^- particle is $\tau_\Xi = (1.639 \pm 0.015) \cdot 10^{-10}$ s. In almost 100% of cases it decays into $\Lambda^0\pi^-$ pairs. The Λ^0 hyperon is also unstable and has a lifetime $\tau_\Lambda = (2.632 \pm 0.020) \cdot 10^{-10}$ s. The most frequent decay channel for this particle is $\Lambda^0 \rightarrow p\pi^-$ (63.90%). The second channel (35.80%) is $\Lambda^0 \rightarrow n\pi^0$ and cannot be studied in the COMPASS detector. The first step in the $\Xi_{3/2}$ pentaquark search focuses on secondary vertices with two outgoing charged particles in order to reconstruct the Λ^0 (Sec. 5.2). Then the reconstructed Λ^0 candidates are combined with π^- particles which do not come from primary vertices. This results in a set of the Ξ^- candidates (Sec. 8). In the last step the reconstructed Ξ^- particles are combined with π^- (in case of $\Xi^{--}_{3/2}$) or π^+ (in case of $\Xi^0_{3/2}$) outgoing from primary vertices (Sec. 9).

Antipentaquarks $\overline{\Theta^+}$ and $\overline{\Xi_{3/2}}$ search is performed in parallel.

3.2 Armenteros plot

The Armenteros plot and the Armenteros variables are very useful in the studies of the "V^0 decays". The "V^0 decay" point is a secondary vertex of no ingoing tracks and of two outgoing tracks of oppositely charged particles. The Armenteros variables are: the transverse momentum of a particle outgoing from a V^0 vertex (p_t) and the asymmetry of the longitudinal momenta of both outgoing particles (p_{asy}):

$$p_t = p_+ sin\phi_+ = p_- sin\phi_- \tag{3.1}$$

$$p_{asy} = \frac{p_{l+} - p_{l-}}{p_{l+} + p_{l-}} \tag{3.2}$$

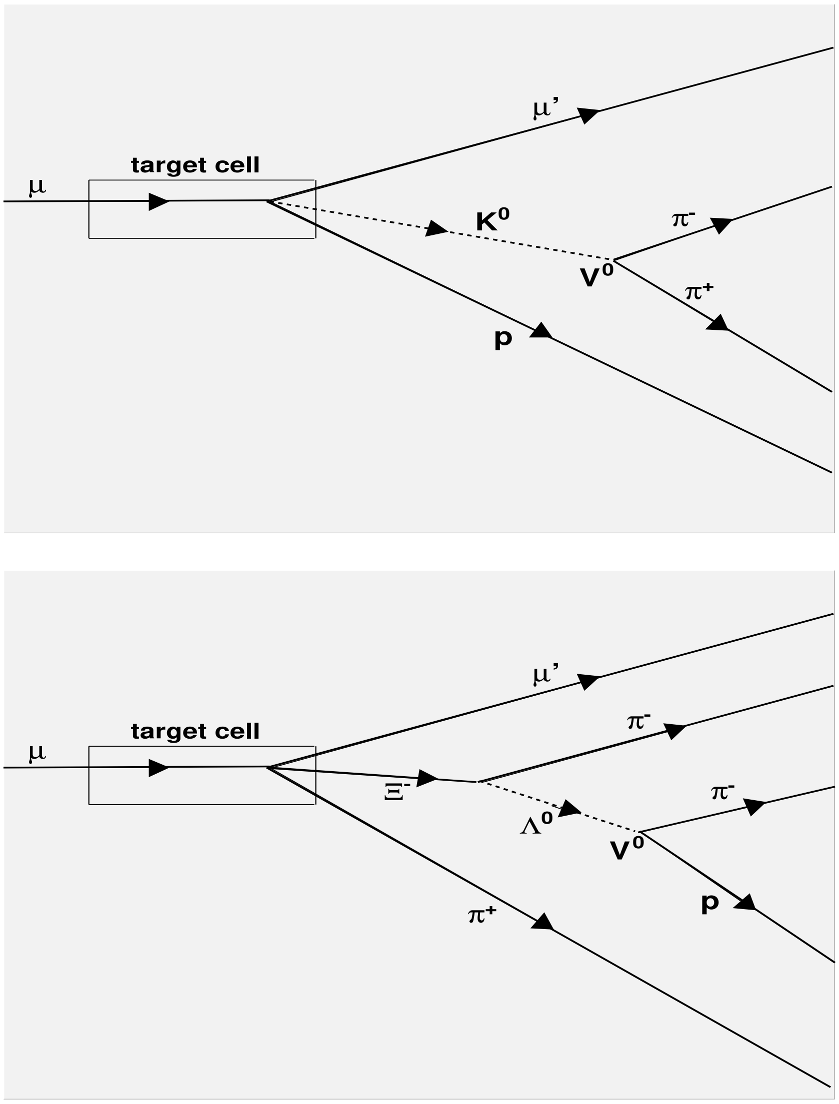

Figure 3.1: Sketches of the Θ^+ (top) and of the $\Xi^0_{3/2}$ decays (bottom). Broken lines mark trajectories of neutral particles.

where:

$$p_{l+} = p_+ cos\phi_+ \tag{3.3}$$

$$p_{l-} = p_- cos\phi_- \tag{3.4}$$

and p_+, p_- are momenta of the positively and negatively charged decay products and ϕ_+ and ϕ_- are the laboratory angles between the decaying particle direction and the directions of the momenta of positive and negative products, respectively.

In Fig. 3.2, p_t versus p_{asy} is plotted. This plot is called the Armenteros plot [17]. V^0 decay vertices of $K^0 \rightarrow \pi^+\pi^-$, $\Lambda^0 \rightarrow p\pi^-$ and $\overline{\Lambda^0} \rightarrow \overline{p}\pi^+$ are clearly visible in the figure. The K^0 events are grouped in the half-ellipse centered at $p_{asy} = 0$. The ellipse ranges from -0.83 to 0.83 in p_{asy} and goes up to 206 MeV in p_t. The Λ^0 and $\overline{\Lambda^0}$ events are distributed along two half-ellipses centered at $p_{asy} = 0.69$ and $p_{asy} = -0.69$, respectively. In p_{asy} ellipses spread ± 0.18 around their centers and in p_t they go up to 101 MeV. In the region of low p_t ($p_t < 35$ MeV) a significant background corresponding to $\gamma \rightarrow e^+e^-$ pair production is present.

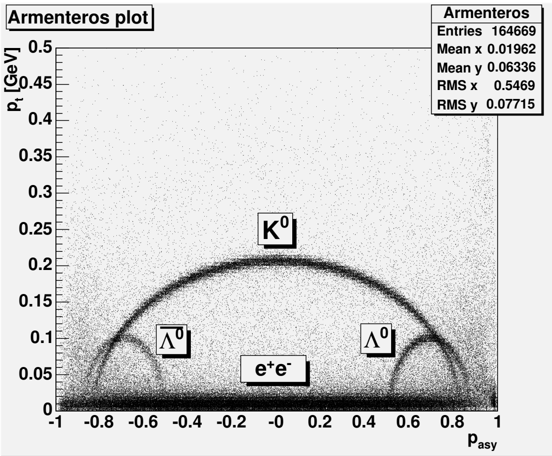

Figure 3.2: Armenteros plot; regions of K^0, Λ^0, $\overline{\Lambda^0}$ decays and e^+e^- pairs production are clearly visible.

3.3 Data

The analysis was performed on the data taken in 2002. Data are divided into several parts called periods. A period corresponds to approximately one week of data taking. Periods are composed of shorter parts called runs. A run is equal to about thirty minutes of the data taking. During 2002, the spectrometer was working with different efficiency. Therefore periods are not of the same length. The number of runs in each period differs from 100 to more than 300. The number of runs from different periods, that were used in this studies, is presented in Table 3.1. Some very short runs were excluded. Therefore the number of runs differs slightly from the total number of runs recorded in each period.

Three periods are marked as transversity periods. It means that polarization of the target in those periods was transverse with respect to the beam direction. This influences the measurement of the spin asymmetries but should not have any impact on the pentaquark production. In the periods marked as 'no RICH', particle identification was not possible because of the RICH malfunction. These periods are excluded in the parts of analysis where the RICH identification of particles is required.

Period	No. of runs	Period	No. of runs
P1C	179	P2E	206
P2A	310	P2F	113
P2B (transversity, no RICH)	140	P2G	192
P2C (transversity, no RICH)	134	P2H (transversity)	170
P2D	178	total:	1622

Table 3.1: Data used for the pentaquark studies.

3.4 Software

Raw data coming from the experiment are recorded and stored in a data base. Events are then reconstructed by CORAL – the COmpass Reconstruction and AnaLysis program. The reconstructed events are grouped in files called miniDST. A software package called PHAST – PHysics Analysis Software Tool – is used for analyzing reconstructed events. In these studies a few versions of PHAST were used: PHAST 5.94, PHAST 5.127, PHAST 6.004 and PHAST 6.008. Differences between those versions do not influence the present analysis. The input files for PHAST are miniDSTs. The output files are ROOT files containing booked histograms which can be viewed and analyzed with ROOT, an Object–Oriented Data Analysis Framework program [18].

Chapter 4

Primary vertex

In this chapter primary vertices are studied. First a description of the main properties of primary interactions is given. Distributions of vertex positions, their multiplicity and of kinematical variables are examined. Then particles decaying in strong interactions, that is in the primary vertex, are analyzed. The emphasis is put on the $\Lambda^0(1520)$ particle since it decays similarly to the Θ^+ pentaquark state. The masses and widths of the signals from different resonances are compared to the Particle Data Group (PDG) values [19].

From now on a COMPASS reference system is used. Its z-axis is along the beam direction, the x-axis is pointing towards the Jura mountains and the y-axis is pointing upwards. The upstream target cell is placed between $z = -100$ cm and $z = -40$ cm. The downstream cell is located between $z = -30$ cm and $z = 30$ cm.

4.1 Primary vertex characteristics

An incident muon may interact inside the target material or in the target vessel, in the spectrometer detectors, and in other materials located in the experimental hall. The target cells are cylinders, 3.0 cm in diameter. Distribution of primary vertices position in the z-axis is presented in Fig. 4.1. In the plot both target cells are clearly visible. Peaks at $z > 50$ cm correspond to interactions in the spectrometer detector planes. The peak at $z = 0$ is an artifact of the reconstruction procedure and does not have any physics meaning. Vertex distribution in the plane perpendicular to the z-axis is shown in Fig. 4.2. The ellipse corresponds to the target centred at $(x, y) = (0, 0)$. In reality the target is shifted by about 0.5–1.5 mm in both x and y directions, as seen in the Fig. 4.2.

Each vertex with a reconstructed incoming muon track is assumed to be a primary vertex. An event may thus contain more than one primary vertex. Events with no primary vertices are discarded from this analysis. In Fig. 4.3 a distribution of the number of reconstructed primary vertices per event is plotted. Over 98.9% of the events, that have primary vertices reconstructed, contain only one such vertex; an admixture of events with more than two primary vertices is negligible small. In Fig. 4.4 a distribution of a number of tracks in a primary vertex is presented. This number is called vertex multiplicity and is calculated excluding the reconstructed outgoing muon. The mean multiplicity is equal to 1.51.

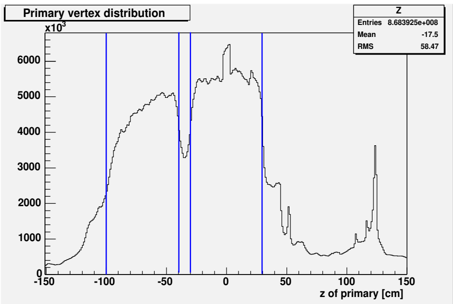

Figure 4.1: Distribution of the primary vertices along the z-axis.

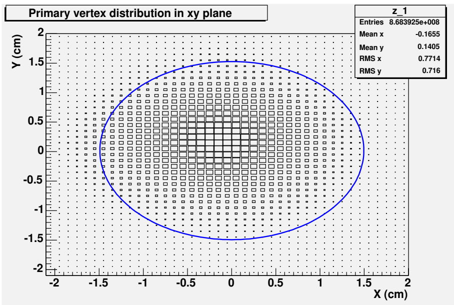

Figure 4.2: Distribution of the primary vertices in the xy plane.

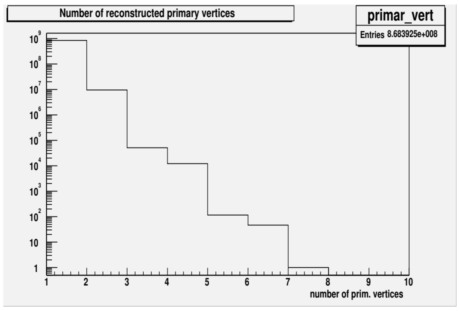

Figure 4.3: Number of primary vertices per event. The logarithmic vertical scale used.

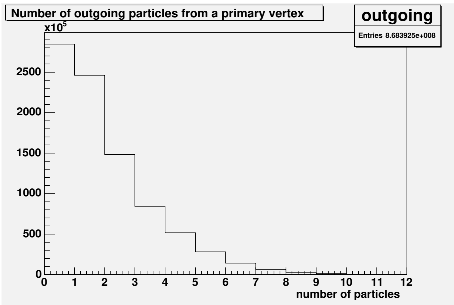

Figure 4.4: Primary vertex multiplicity (outgoing muon excluded).

4.2 Kinematical variables x, y and x_F

A diagram illustrating the inelastic muon-nucleon scattering is presented in Fig. 4.5.

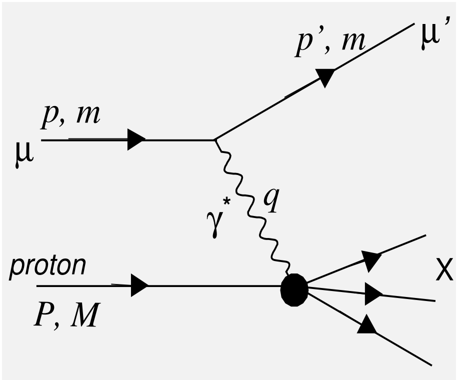

Figure 4.5: Inelastic scattering process. Symbols are explained in the text.

Here P and M stand for the nucleon four-momentum and nucleon mass, while p, p' and m describe incident and scattered muon four-momenta and the muon mass. The four-momentum transfer between the muon and the nucleon is denoted by q. The transfer occurs *via* the exchange of a virtual photon. Two variables are very useful in the description of the inelastic μN scattering: x and y. The Bjorken scaling variable x is defined as:

$$x = \frac{-q^2}{q \cdot P} = \frac{-q^2}{2M\nu} \tag{4.1}$$

where ν is the muon energy loss in the nucleon rest frame. The variable y is a fraction of the muon energy loss in the nucleon rest frame:

$$y = \frac{q \cdot P}{p \cdot P} = \frac{\nu}{E} \tag{4.2}$$

where E is the incoming muon energy. Distributions of x and y in the COMPASS 2002 data are presented in Fig. 4.6 and 4.7. Shapes of the distributions result from a reaction dynamics and from the acceptance of the detector. In particular in Fig. 4.6 a strong peak at x equal to about 1/2000 corresponds to scattering of the muons off atomic electrons.

The Feynmann variable – x_F – is a variable useful in the hadron spectroscopy. It is defined as:

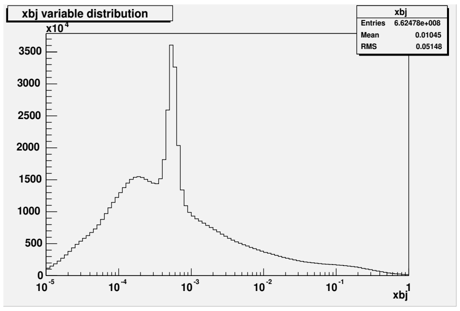

Figure 4.6: Distribution of the scaling variable x.

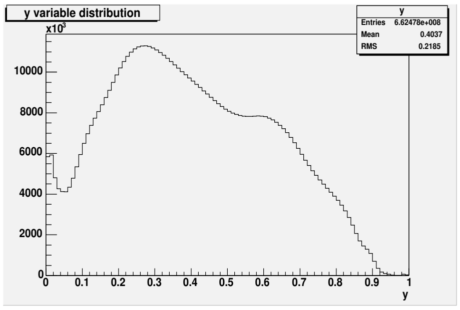

Figure 4.7: Distribution of the $y = \nu/E$ variable.

$$x_F = \frac{p_{h\gamma}}{\sqrt{s}} \tag{4.3}$$

where $p_{h\gamma}$ is the produced hadron momentum along the direction parallel to the direction of a virtual photon and $\sqrt{s}$ is the invariant mass of photon-nucleon system.

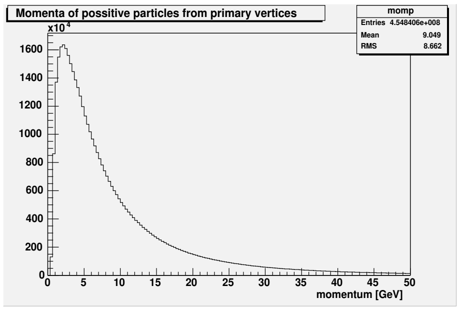

Figure 4.8: Distribution of the momenta of positive particles outgoing from the primary vertex.

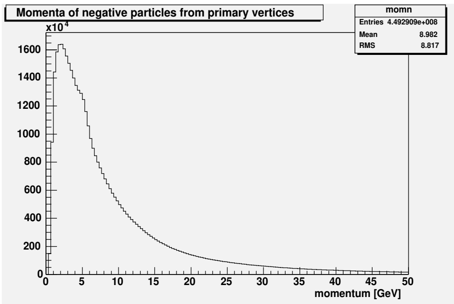

Figure 4.9: Distribution of the momenta of negative particles outgoing from the primary vertex.

4.3 Identification of particles outgoing from a primary vertex

Most of the detectable tracks of hadrons outgoing from a primary vertex correspond to pions, kaons and protons. Momenta of these particles can be measured in SAS and LAS. In Figs 4.8 and 4.9 distributions of momenta of positive and negative particles outgoing from a primary vertex are plotted. A bump in the range 4–7 GeV in Fig. 4.9 is due to atomic electrons knocked out from the target. Identification of particles is done by the RICH. Efficiency of the identification, presently still quite low, is a function of a particle momentum and its type – π, K and p can be identified if their momenta exceed 2.5 GeV, 9 GeV and 17 GeV, respectively. The particles can be identified up to about 50 GeV. Momentum distributions of π, K and p identified in the RICH are presented in Figs 4.10, 4.12, 4.14 (for positive particles) and in Figs 4.11, 4.13, 4.15 (for negative particles). The identification of particles is performed basing on the numerical procedure written by Yann Bedfer [20].

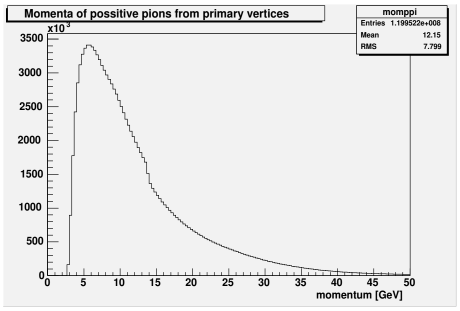

Figure 4.10: π^+ momenta distribution.

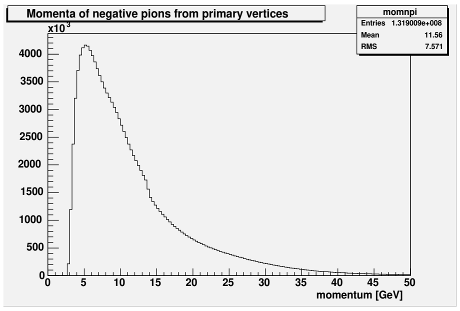

Figure 4.11: π^- momenta distribution.

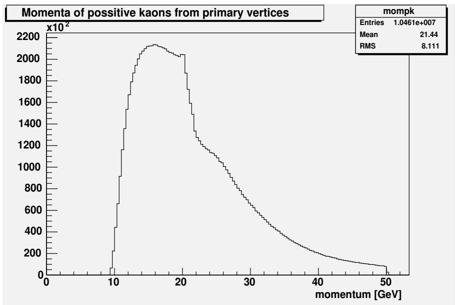

Figure 4.12: K^+ momenta distribution.

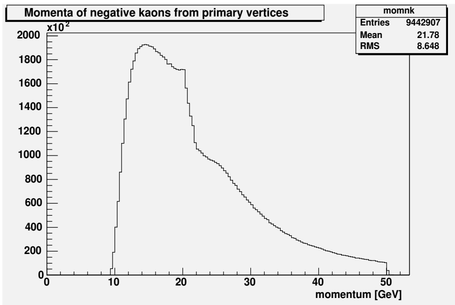

Figure 4.13: K^- momenta distribution.

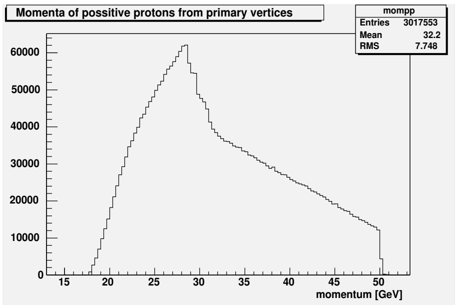

Figure 4.14: p momenta distribution.

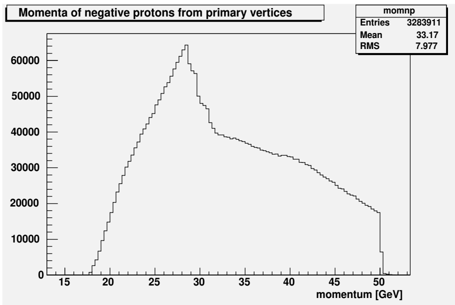

Figure 4.15: $\overline{p}$ momenta distribution.

4.4 Two-body strong decays of baryons and mesons

A particle decaying *via* strong interactions has a mean life time shorter than about 10^{-20} s. Thus it decays very close to a primary vertex. In the reconstruction procedure the particle decay products are attributed to that vertex. Therefore distributions of invariant masses of pairs of tracks outgoing from the interaction point should reveal the existence of short living states. In this section distributions of the invariant masses of $\pi^+\pi^-$, $K^+\pi^-$, $K^-\pi^+$, K^+K^-, $p\pi^-$, $\overline{p}\pi^-$, pK^-, $\overline{p}K^+$, $p\pi^+$ and $\overline{p}\pi^+$ systems where both particles were identified by RICH will be presented. Apart from the particles decaying *via* strong interactions a small admixture of states decaying *via* weak interactions is observed in a reconstructed primary vertex.

4.4.1 Results for mesons

Heavy mesons produced in a primary vertex can decay into charged pions or kaons. In Fig. 4.16 an invariant mass distribution of pairs of oppositely charged pions is plotted. Arrows mark positions of four known states.

The bump at the mass of about 498 MeV corresponds to K^0 particles. These particles decay *via* weak interactions. Therefore most of them decay far enough from the primary vertices to produce detectable secondary vertices. Nevertheless some of them decay very close to a primary interaction point and during reconstruction products of their decays are ascribed to it. The K^0 meson will be discussed in Sec. 5.1.

Second bump corresponds to the $\rho(770)$ state. It is approximated by a sum of a Gaussian and an exponential functions (Fig. 4.17). The Gaussian is centered at (757.77 ± 0.13) MeV and its standard deviation is (48.32 ± 0.22) MeV. Corresponding PDG values for the $\rho(770)$ are: mass equal to (771.1 ± 0.9) MeV and FWHM equal to (149.2 ± 0.7) MeV. For the explanation of a $\rho(770)$ distribution shape see [21].

The next bump is located in the mass range of (950–1020) MeV (Fig. 4.18). To the range of (900–1100) MeV a sum of a Gaussian and an exponential functions is fitted. The Gaussian is centered at (972.6 ± 1.0) MeV and has a standard deviation of (19.8 ± 1.0) MeV. It may correspond to the $f_0(980)$ meson which has a PDG mass of (980 ± 10) MeV and FWHM of (40–100) MeV.

A sum of a Gaussian and an exponential functions is also fitted to the data in the range of (1100–1500) MeV (Fig 4.19). This Gaussian function is centered at (1256.0 ± 1.1) MeV and has a standard deviation of (68.9 ± 1.3) MeV and probably corresponds to another meson – $f_2(1270)$. It has a PDG mass of (1275.4 ± 1.2) MeV and FWHM of $185.1^{+3.4}_{-2.6}$ MeV.

In the region (900–1600) MeV several resonances decaying into $\pi^+\pi^-$ may give contributions to the observed $f_0(980)$ and $f_2(1270)$ bumps. These resonances are: $\eta'(958)$, $\phi(1020)$, $f_0(1370)$, $\rho(1450)$, $f_0(1500)$, $f_2'(1525)$. The bumps can also be produced by kinematical reflections coming from three or more body decays which are not studied in this work.

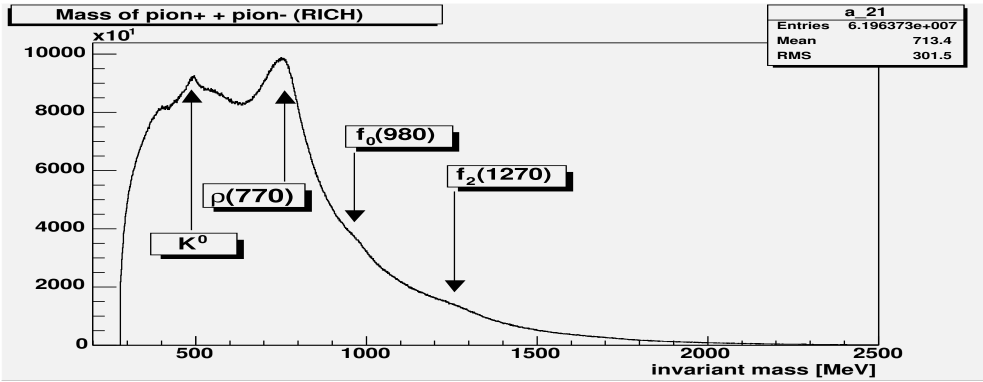

Figure 4.16: Distribution of the invariant mass of $\pi^+\pi^-$ pairs.

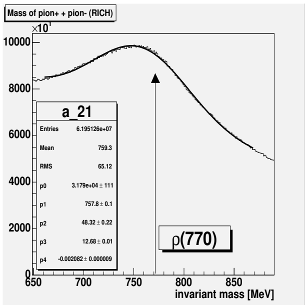

Figure 4.17: $\rho(770)$ zoom of Fig. 4.16

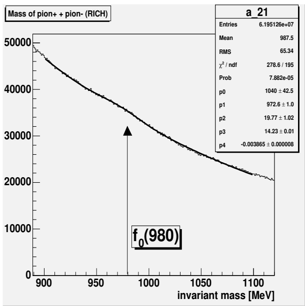

Figure 4.18: $f_0(980)$ zoom of Fig. 4.16

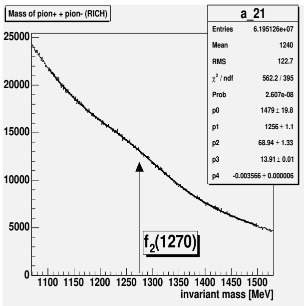

Figure 4.19: $f_2(1270)$ zoom of Fig. 4.16

In Figs 4.20 and 4.23 invariant masses of $K^+\pi^-$ and $K^-\pi^+$ systems are plotted. Both plots reveal two bumps. To the first bump a sum of a Gaussian and a second degree polynomial functions is fitted. The other bump is approximated by a sum of a Gaussian and an exponential functions.

The Gaussian functions describing the first bump are centered at the masses equal to (896.80 ± 0.20) MeV and (897.22 ± 0.27) MeV in $K^+\pi^-$ and $K^-\pi^+$ mass spectra, respectively. Their standard deviations are (24.08 ± 0.25) MeV and (23.68 ± 0.34) MeV. The bumps correspond to $K^*(892)$ and $\overline{K^*}(892)$ states. These states have a PDG mass value of (896.10 ± 0.26) MeV and FWHM of (50.7 ± 0.6) MeV.

Other bumps in the $K^+\pi^-$ and $K^-\pi^+$ mass spectra are described by the Gaussian functions centered at the masses (1420.1 ± 2.1) MeV and (1420.6 ± 2.5) MeV, respectively. Their standard deviations are equal to (53.0 ± 2.5) MeV and (57.2 ± 3.0) MeV. The bumps correspond to $K_2^*(1430)$ and $\overline{K_2^*}(1430)$ states for which the PDG values are: the mass of (1432.4 ± 1.3) MeV and FWHM of (109 ± 5) MeV.

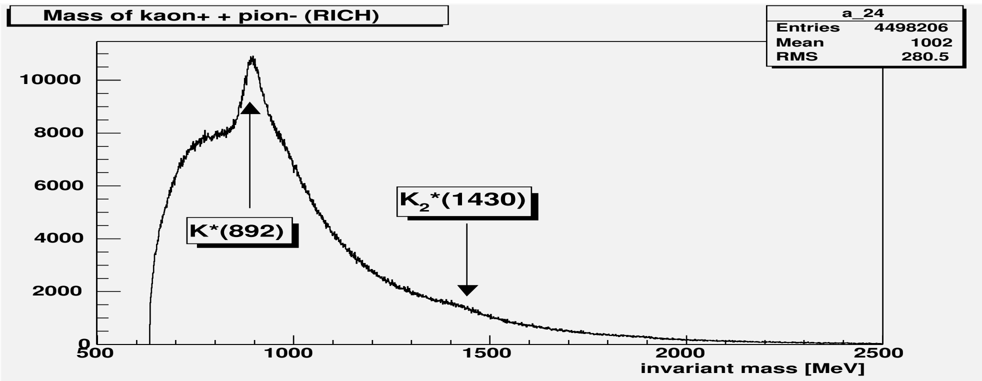

Figure 4.20: $K^+\pi^-$ invariant mass distribution.

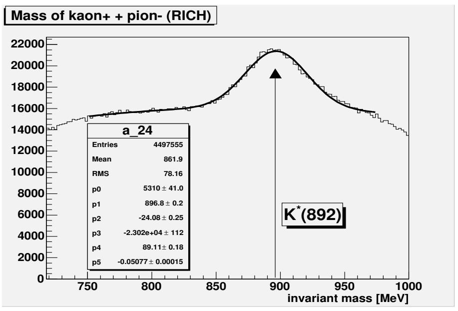

Figure 4.21: $K^*(892)$ zoom of Fig. 4.20

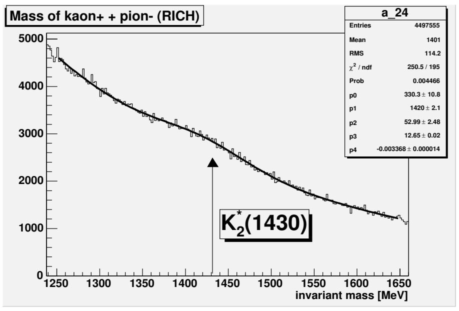

Figure 4.22: $K_2^*(1430)$, zoom of Fig. 4.20

In Fig. 4.26 an invariant mass of K^+K^- system is plotted. A narrow signal of $\phi(1020)$ particle is clearly visible. A sum of a Gaussian and a second degree polynomial functions results in a Gaussian centered at (1119.68 ± 0.03) MeV with a standard deviation of (4.04 ± 0.03) MeV. The PDG values for $\phi(1020)$ are: the mass equal to (1119.456 ± 0.020) MeV and FWHM of (4.26 ± 0.05) MeV.

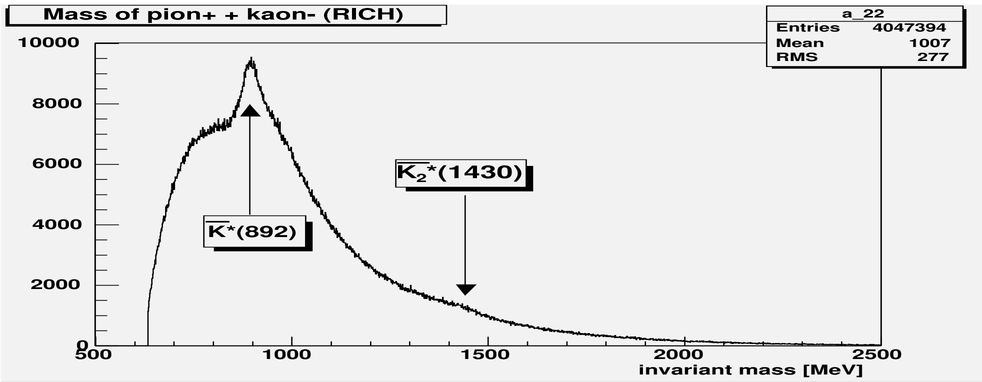

Figure 4.23: $K^-\pi^+$ invariant mass distribution.

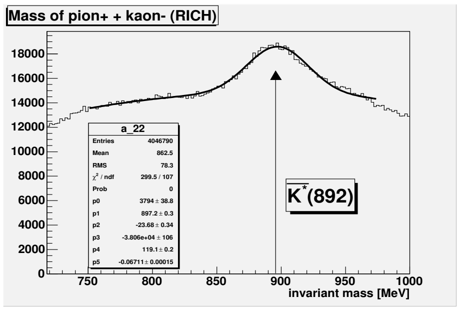

Figure 4.24: $\overline{K^*}(892)$, zoom of Fig. 4.23

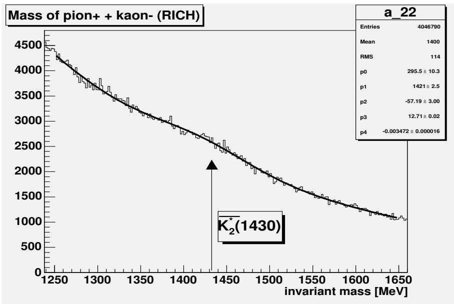

Figure 4.25: $\overline{K_2^*}(1430)$, zoom of Fig. 4.23

4.4.2 Results for non strange baryons

In Figs 4.27–4.30 the invariant masses of $p\pi^-$, $\overline{p}\pi^+$, $p\pi^+$ and $\overline{p}\pi^-$ systems are presented. Vertical lines indicate masses where $\Delta(1232)$ particles should be visible. The signals are not present in the plots. However the background in the region of 1200–1400 MeV has its maximum and wide bumps (FWHM of $\Delta(1232)$ is equal 120 MeV) can be masked by the background.

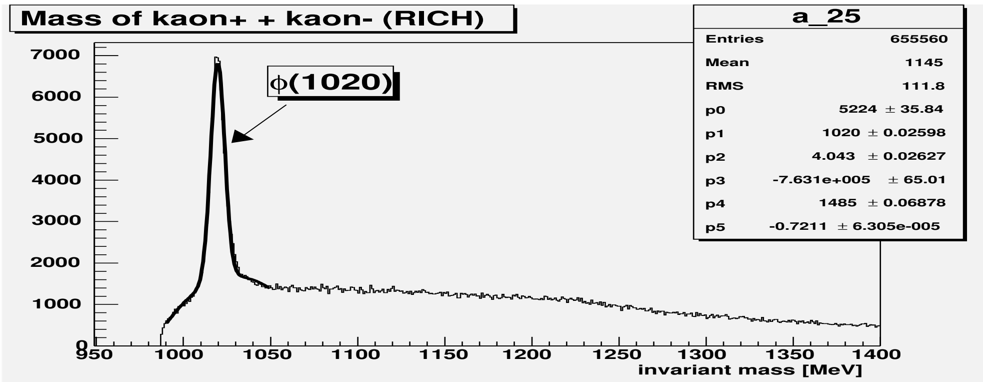

Figure 4.26: K^-K^+ invariant mass distribution.

4.4.3 $\Lambda^0(1520)$ studies

The mass of a $\Lambda^0(1520)$ particle is very close to the mass of the Θ^+ pentaquark state. Also the $\Lambda^0(1520)$ decay channel (into pK^-) is similar to the Θ^+ decay channel (pK^0). Therefore $\Lambda^0(1520)$ particle can give an insight into phase space limits of the Θ^+ decays in the COMPASS detector. The pK^- and $\overline{p}K^+$ invariant mass distributions reveal some structures in the range of 1490–1600 MeV (Fig. 4.31) which may correspond to the $\Lambda^0(1520)$ and $\overline{\Lambda^0}(1520)$ states. However due to a possible RICH modification of the spectrum, estimation of the number of particles is impossible. It is worth noticing that in the low energy experiments where the Θ^+ signal is observed the $\Lambda^0(1520)$ particle is also clearly visible [5,8].

4.4.4 Reconstruction of particles without RICH identification

RICH is sensitive only to particles from a defined momentum range, different for different kinds of particles (see Sec. 4.3). Even inside the appropriate range, the RICH efficiency is far below 100%. This means that the identification is accompanied by a significant loss of data. It may also happen that particles from a decay of certain states are produced with small momenta and thus cannot be identified in the RICH. Such decays cannot be analysed with the RICH identification. In Figs 4.32–4.35 invariant mass distributions of $\pi^+\pi^-$, K^+K^-, $K^-\pi^+$ and $K^+\pi^-$ systems are plotted. The plots are obtained without a demand of RICH identification; the particles are assumed to be pions or kaons. In the plots only the strongest signals remain: $\rho(770)$, $\phi(1020)$, $\overline{K^*}(892)$, $K^*(892)$.

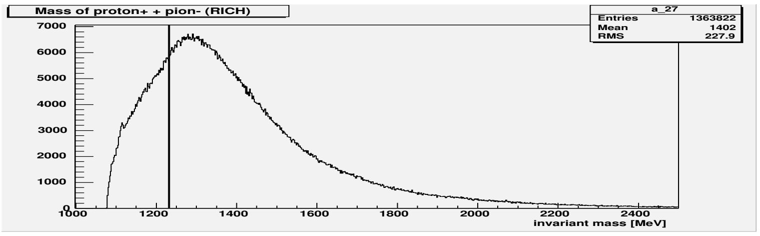

Figure 4.27: $p\pi^-$ invariant mass distribution.

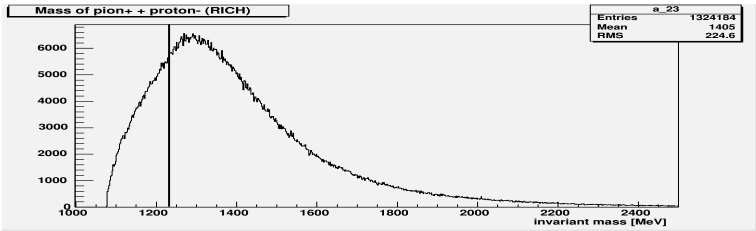

Figure 4.28: $\overline{p}\pi^+$ invariant mass distribution.

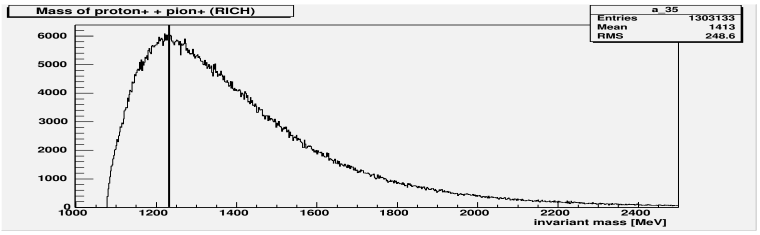

Figure 4.29: $p\pi^+$ invariant mass distribution.

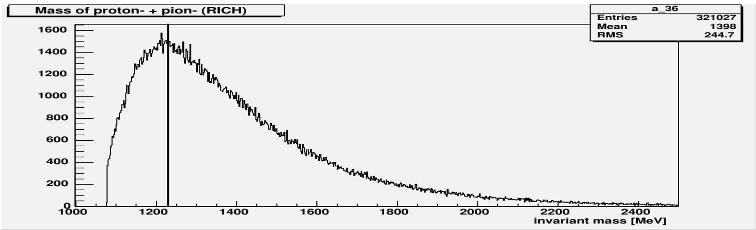

Figure 4.30: $\overline{p}\pi^-$ invariant mass distribution.

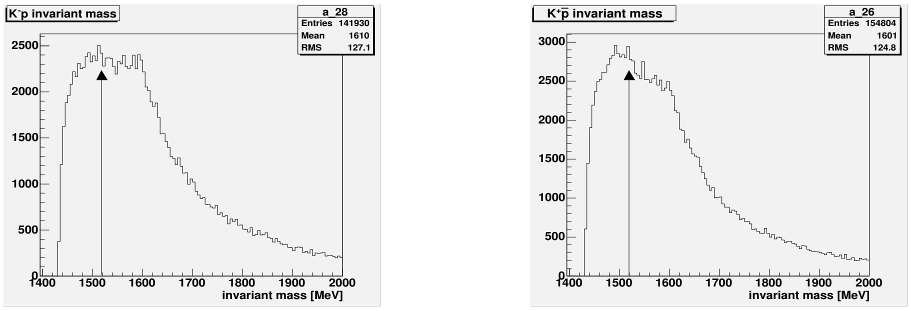

Figure 4.31: Distributions of the pK^- (left) and $\overline{p}K^+$ (right) masses. Arrows indicate 1520 MeV value.

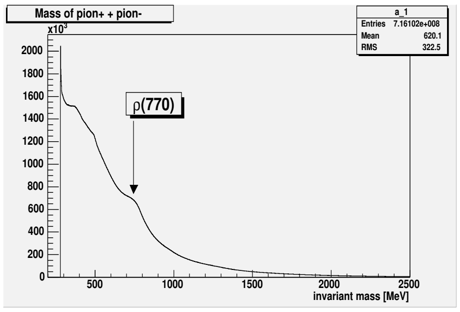

Figure 4.32: $\pi^+\pi^-$ invariant mass distribution (without identification).

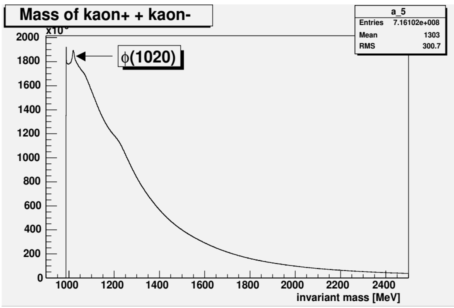

Figure 4.33: K^+K^- invariant mass distribution (without identification).

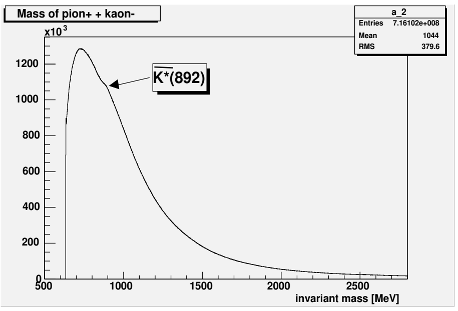

Figure 4.34: $K^-\pi^+$ invariant mass distribution (without identification).

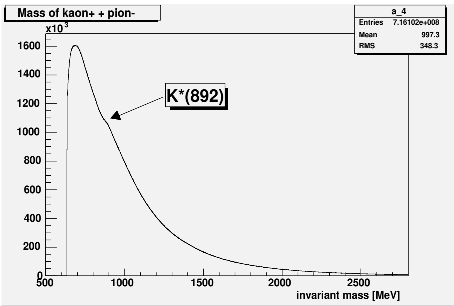

Figure 4.35: $K^+\pi^-$ invariant mass distribution (without identification).

4.5 Event selection based on characteristics of primary vertices

For the pentaquark search two initial criteria connected with primary vertices are applied. These criteria are:

- An event must contain exactly one primary vertex (1.1% events containing primary vertices have more than one primary vertex).
- The primary vertex is located inside geometrical limits of the target in the z-axis as well as in the xy-plane (the target shifts in x and y described in Sec. 4.1 are not taken into account).

The first cut is needed to simplify the analysis and the second one rejects interactions that take place outside the target area.

Chapter 5

Studies of V^0 vertices

A secondary vertex of a "V^0" type is registered in the detector when a chargeless particle decays into two particles of opposite signs. Examples are decays of K^0 mesons and Λ^0 hyperons. A decaying state is called a V^0 particle. To distinguish between primary and secondary vertices the decay must occur far enough from the primary interaction point. In this chapter cuts leading to the best selection of the K^0 and Λ^0 samples are discussed. The sample is characterized by two variables, that is by the signal (S) defined as the number of events above the background and by the signal-to-background ratio (S/B) which represents the purity of the sample. The larger are those numbers the better selected is the sample. If the signal-to-background ratio is small, a possible pentaquark peak may be hidden by a strong background. If a number of Θ^+ candidates is low, the peak significance would not be meaningful. Therefore an important part of the pentaquark analysis is a selection of the best K^0 and Λ^0 samples.

In COMPASS, studies of the V^0 particles are done for calibration purpose, cf. [22, 23]. In the analysis presented in this section certain cuts originating from those studies are employed.

The first step of the V^0 analysis is the search for secondary vertices with two outgoing particles of opposite signs. For K^0 studies it is assumed that both particles are pions. In case of Λ^0 a positive particle is assumed to be a proton and a negative – a pion (for $\overline{\Lambda^0}$ the opposite is assumed). Particle momenta are reconstructed from the information registered by several tracking detectors located in front of and behind the SAS and LAS magnets.

In what follows, V^0 mass distributions will denote distributions of differences between the reconstructed and nominal masses of V^0 particles. This means that for unbiased samples all such distributions should have Gaussian shapes centered around zero.

5.1 K^0 selection

To obtain the best K^0 signal the following cuts are imposed:

- An event has a secondary V^0 vertex for which $z_{V^0} > 56$ cm.
- The $\Delta\theta$ angle for a V^0 particle is smaller than 0.01 radians, where $\Delta\theta$ is an angle between the momentum vector of the reconstructed V^0 and the straight line connecting the primary and the V^0 vertices.
- p_t of a particle from a V^0 decay is greater than 23 MeV to reject the e^+e^- pairs (see Fig. 3.2).
- p_t is not in the range 90–115 MeV. This cut removes an admixture of Λ^0 and $\overline{\Lambda^0}$ hyperons (see Fig. 3.2).
- χ^2 of the reconstructed V^0 vertex is smaller than 2.

The cuts are described in the following subsections. In all cases two Gaussian functions are fitted to the K^0 mass distributions (in the case where no cuts are imposed one Gaussian function is fitted, cf. Fig. 5.1). A background is assumed to be described by a second degree polynomial. The signals and the signal-to-background ratios are calculated in the ± 18 MeV mass windows centred at the nominal (PDG) K^0 mass value (in the case where no cuts are imposed a mass window is equal to ± 21 MeV).

5.1.1 Cut on z_{V^0}

Demand that a V^0 vertex must be located outside the target reduces significantly the background and improves the signal-to-background ratio. The background inside the target area arises mainly due to the errors in the reconstruction process which result from a multiple Coulomb scattering of the decay products inside the target material. Efficiencies of different z_{V^0} cuts are illustrated in Table 5.1. In Figs 5.1 and 5.2 the K^0 mass distributions without and with $z_{V^0} > 56$ cm cut are plotted. The cut on $z_{V^0} > 56$ corresponds to the V^0 vertices located outside the target vessel.

5.1.2 Cut on $\Delta\theta$ angle

All K^0 particles originate from a primary vertex unless there is another, not recorded, primary vertex, or there is a secondary interaction caused by a neutral particle. A cut on the $\Delta\theta$ rejects the K^0 candidates which may not come from the primary vertex. These K^0 candidates are mainly random combinations of tracks or a real K^0 particles suffering from a bad secondary vertex reconstruction. In Table 5.2 signal-to-background ratios for different cuts on $\Delta\theta$ are presented. In Fig. 5.3 a K^0 mass distribution with the cut on $\Delta\theta < 0.01$ radians is plotted.

Cut [cm]	S	S/B	Cut [cm]	S	S/B
no cut	5 744 319	0.09	**>56**	**2 449 577**	**2.03**
>30	3 739 512	1.16	>60	2 271 276	2.09
>40	3 195 286	1.64	>70	1 832 295	2.08
>50	2 729 762	1.87	>80	1 458 060	1.99

Table 5.1: The K^0 signals and S/B ratios for different z_{V^0} cuts. The cut in bold is used in the analysis

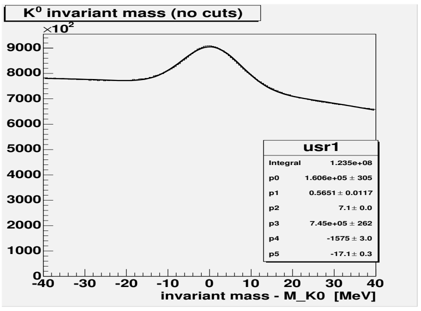

Figure 5.1: K^0 mass distribution (no cuts).

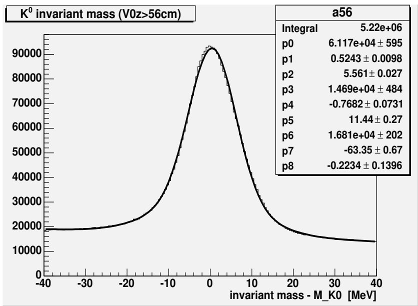

Figure 5.2: K^0 mass distribution ($z_{V^0} > 56$ cm).

5.1.3 Cuts on p_t

Rejection of V^0 with $p_t < 23$ MeV and with p_t in the interval (90–115) MeV removes from the sample the $\gamma \to e^+e^-$ background as well as Λ^0, $\overline{\Lambda^0}$ hyperons. In Fig. 5.4 a K^0 mass distribution with the cuts on p_t is plotted. The number of signal events is 2 089 892, while the signal-to-background ratio is equal to 7.01.

Cut [rad]	Signal	S/B	Cut [rad]	Signal	S/B
<0.1	2 461 601	2.11	<0.02	2 368 150	3.14
<0.07	2 464 559	2.25	**<0.01**	**2 241 387**	**3.78**
<0.05	2 456 958	2.44	<0.005	2 071 718	4.45
<0.03	2 413 707	2.78			

Table 5.2: The K^0 signals and S/B ratios for different $\Delta\theta$ cuts ($z_{V^0} > 56$ cm cut). The cut in bold is used in the analysis.

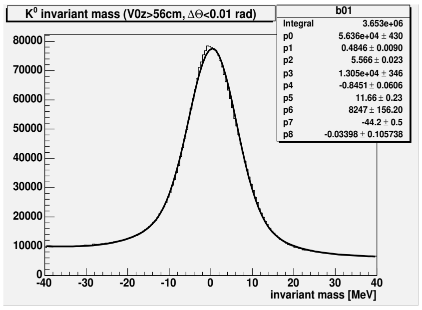

Figure 5.3: K^0 mass distribution ($\Delta\theta < 0.01$ rad, $z_{V^0} > 56$ cm).

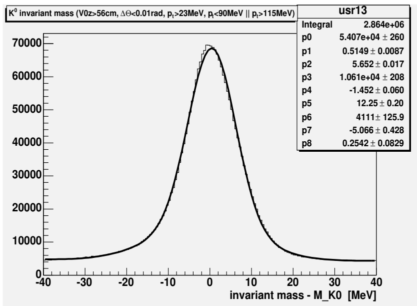

Figure 5.4: K^0 mass distribution (p_t cuts, $\Delta\theta < 0.01$ rad, $z_{V^0} > 56$ cm).

5.1.4 Cut on χ^2 value

A χ^2 value is associated with each reconstructed vertex and describes the goodness of its reconstruction. Vertices with larger χ^2 are more likely to suffer from a bad reconstruction. Table 5.3 shows efficiencies of different cuts on χ^2 of the V^0 vertex. Invariant mass distribution of K^0 candidates with $\chi^2 < 2$ cut is presented in Fig. 5.5.

Cut	S	S/B	Cut	S	S/B
<6.0	2 038 359	7.01	<1.5	1 711 397	9.87
<4.0	1 976 255	8.39	<1.0	1 561 429	10.50
<2.0	**1 804 620**	**9.42**			

Table 5.3: The K^0 signals and S/B ratios for different cuts on the χ^2 of the V^0 vertex ($z_{V^0} > 56$ cm, $\Delta\theta < 0.01$ rad, $p_t > 23$ MeV, $p_t < 90$ MeV or $p_t > 115$ MeV cuts). The cut in bold is used in the analysis.

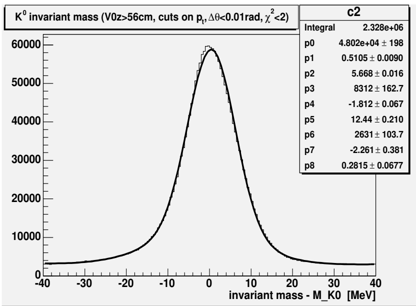

Figure 5.5: K^0 mass distribution ($\chi^2 < 2$, p_t cuts, $\Delta\theta < 0.01$ rad, $z_{V^0} > 56$ cm).

5.1.5 Cuts on RICH identification

The demand that one or both pions were identified in the RICH detector is a criterion which should greatly improve the signal-to-background ratio. This indeed is the case but at the expense of a significant reduction of statistics. In Figs 5.6–5.7 and in Table 5.4 the cuts on RICH identification are summarized. RICH identification of pions will not be used in the pentaquark analysis.

Cut	S	S/B
one pion identified	1 032 080	23.79
both pions identified	306 349	92.52

Table 5.4: The K^0 signals and S/B ratios with a demand that one or both pions are identified in RICH ($z_{V^0} > 56$ cm, $\Delta\theta < 0.01$ rad, $p_t > 23$ MeV, $p_t < 90$ MeV or $p_t > 115$ MeV, $\chi^2 < 2$ cuts).

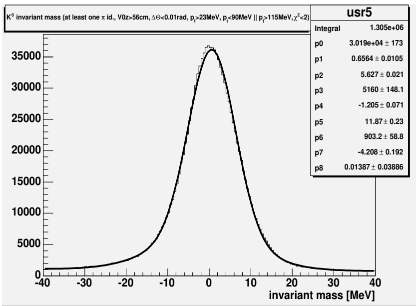

Figure 5.6: K^0 mass distribution with at least one pion identified ($\chi^2 < 2$, p_t cuts, $\Delta\theta < 0.01$ rad, $z_{V^0} > 56$ cm cuts).

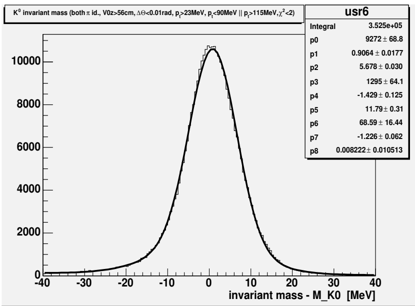

Figure 5.7: K^0 mass distribution with both pions identified ($\chi^2 < 2$, p_t cuts, $\Delta\theta < 0.01$ rad, $z_{V^0} > 56$ cm cuts).

5.1.6 Discussion of the K^0 signal

The cuts mentioned in sections 5.1.1–5.1.4 were optimized to obtain the best signal-to-background ratio without loosing too many K^0 particles (see Table 5.5). A closer examination of the K^0 mass distributions (Figs 5.2–5.7) reveal a small bump in the range of (-2–0) MeV. It is due to a class of events which contain V^0 vertices located at z greater than 200 cm. This class of events is described in [22]. During different running periods various detectors were switched off or were working with changing efficiencies and alignments. Therefore the K^0 mass distributions are not exactly the same in each of the periods and it is not possible to fit a single Gaussian function to the K^0 signal in the summed data. Therefore a sum of two Gaussian functions and a second degree polynomial are chosen to describe the K^0 signal and the background respectively.

Cut	S	Relative S [%]	S/B	Relative S/B
no cuts	5 744 319	100.0	0.09	1.0
$z_{V^0} > 56$ cm	2 449 577	42.6	2.03	22.6
$\Delta\theta < 0.01$ rad	2 241 387	39.0	3.78	42.0
cuts on p_t	2 089 892	36.4	7.01	77.9
$\chi^2 < 2$	1 804 620	31.4	9.42	104.7

Table 5.5: Final cuts for the K^0 selection.

5.2 Λ^0 selection

In order to obtain clean Λ^0 and $\overline{\Lambda^0}$ signals the following cuts are imposed on V^0 events:

- An event has a secondary V^0 vertex for which $z_{V^0} > 56$ cm.
- p_t of a particle from a V^0 decay is greater than 23 MeV to reject the e^+e^- pairs (see Fig. 3.2).
- Mass of the V^0 has a value outside the ± 12 MeV window around the nominal K^0 mass. Here the V^0 mass is calculated under the assumption that both particles from the V^0 decay are pions.
- χ^2 of the reconstructed V^0 vertex is smaller than 2.
- $|\cos(\overline{p^*_\Lambda}, \overline{p^*_\pi})| < 0.90$. This cut suppresses an admixture of decaying particles of spin quantum number different from 1/2.

The reasons for using cuts on z, p_t and χ^2 are the same as in the case of K^0 analysis (see Sec. 5.1). The cut on $\Delta\theta$ (see Sec. 5.1.2) is not used because the $\Xi_{3/2}$ pentaquark analysis focus on the Λ^0 ($\overline{\Lambda^0}$) coming from Ξ^- ($\overline{\Xi^-}$) decays and not directly from the primary vertices. The above cuts are described in the following subsections. In all cases two Gaussian functions are fitted to the Λ^0 mass distributions (in the case where no cuts are imposed one Gaussian function is fitted). A background is assumed to be described by a second degree polynomial. The signals and signal-to-background ratios are calculated in the ± 8 MeV mass windows centred at the nominal (PDG) Λ^0 mass value.

5.2.1 Cut on z_{V^0}

The results of different z_{V^0} cuts are presented in Table 5.6. In Fig. 5.8 Λ^0 and $\overline{\Lambda^0}$ mass distributions without cuts on z_{V^0} are plotted. The same distributions but with a demand that $z_{V^0} > 56$ cm are presented in Fig. 5.9. For more details on z_{V^0} cuts see Sec. 5.1.1.

5.2.2 Cut on p_t

The Λ^0 and $\overline{\Lambda^0}$ mass distributions after cuts on $p_t > 23$ MeV are presented in Fig. 5.10. The signals are 482 262 and 272 813 events while the signal-to-background ratios are 0.82 and 0.52, respectively. It can be noticed that the signals are slightly greater than in the samples without p_t cut. This is caused by the change in the shape of the background on the left side of Λ^0 and $\overline{\Lambda^0}$

peaks (compare Figs 5.9 and 5.10), which results in a substantial change in the parameters of the fitted functions.

	Λ^0		$\overline{\Lambda^0}$	
Cut [cm]	S	S/B	S	S/B
no cut	920 022	0.05	463 267	0.03
>30	720 862	0.35	387 270	0.19
>40	619 597	0.44	336 970	0.24
>50	533 698	0.49	294 353	0.28
>56	**480 017**	**0.54**	**267 393**	**0.30**
>60	446 914	0.56	250 936	0.32
>70	368 370	0.62	198 095	0.33
>80	300 310	0.67	162 204	0.36

Table 5.6: The Λ^0, $\overline{\Lambda^0}$ signals and S/B ratios for different z_{V^0} cuts. The cut in bold is used in the analysis.

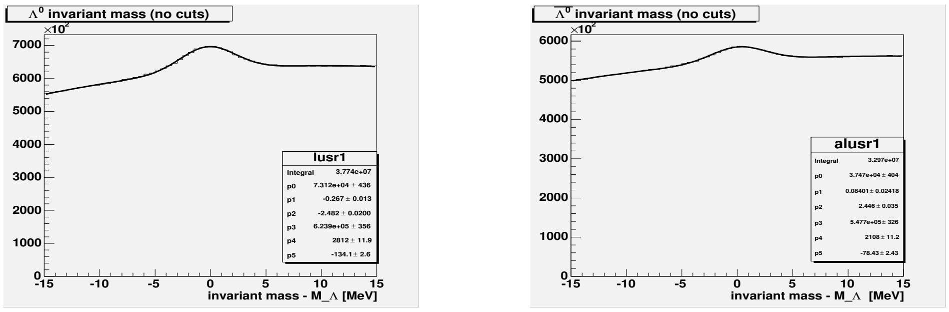

Figure 5.8: Λ^0 (left) and $\overline{\Lambda^0}$ (right) mass distributions (no cuts).

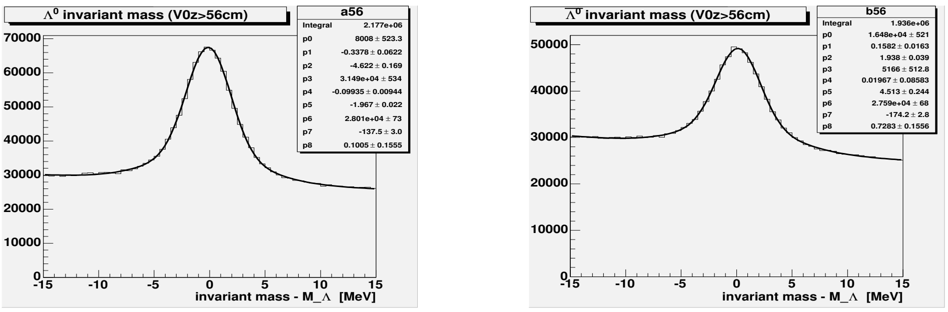

Figure 5.9: Λ^0 (left) and $\overline{\Lambda^0}$ (right) mass distributions ($z_{V^0} > 56$ cm).

5.2.3 Removing the K^0 admixture

To remove the admixture of K^0 particles from the Λ^0 and $\overline{\Lambda^0}$ samples the following procedure is used. It is assumed that both tracks outgoing from a V^0 vertex are pions and a mass of a V^0 particle is calculated under this assumption. If this mass is in the ± 12 MeV window centred at the nominal K^0 mass value then such a V^0 candidate is rejected. After this cut 429 436 Λ^0 and 246 347 $\overline{\Lambda^0}$ candidates remain. The signal-to-background ratios are 0.91 and 0.59, respectively. The invariant mass distributions are presented in Fig. 5.11.

5.2.4 Cut on χ^2

In Table 5.7 efficiencies of different cuts on χ^2 value of the V^0 vertex are collected. In Fig. 5.12 Λ^0 and $\overline{\Lambda^0}$ signals with cut on $\chi^2 < 2$ are plotted. For more details on χ^2 cut see Sec. 5.1.4.

	Λ^0		$\overline{\Lambda^0}$	
Cut	S	S/B	S	S/B
< 6.0	417 687	1.00	239 613	0.66
< 4.0	402 906	1.09	231 006	0.71
< 2.0	**367 537**	**1.25**	**210 001**	**0.81**
< 1.5	348 488	1.31	198 701	0.85
< 1.0	318 088	1.39	180 420	0.89

Table 5.7: The Λ^0, $\overline{\Lambda^0}$ signals and S/B ratios for different cuts on the χ^2 of the V^0 vertex ($z_{V^0} > 56$ cm, $p_t > 23$ MeV, rejection of K^0 particles). The cut in bold is used in the analysis.

5.2.5 Cut on $\pi\Lambda^0$ angle

The Λ^0 particle has a spin quantum number equal to 1/2. It decays into a $p\pi$ pair. In the Λ^0 rest frame a distribution of a $\cos(\overline{p^*_\Lambda}, \overline{p^*_\pi})$, where $\overline{p_\pi}$ and $\overline{p_\Lambda}$ denote a pion and a Λ^0 momentum vectors respectively, is flat. In Fig. 5.13 the distributions of $\cos(\overline{p^*_\Lambda}, \overline{p^*_\pi})$ for Λ^0 and $\overline{\Lambda^0}$ are presented. Strong peaks at +1 and -1 are clearly visible. These peaks do not correspond to the decays of 1/2 spin particles. Therefore the events from the peaks should be removed from the sample. In Table 5.9 signals with different $|\cos(\overline{p^*_\Lambda}, \overline{p^*_\pi})|$ cuts are presented. Fig. 5.14 shows the invariant mass distributions with $|\cos(\overline{p^*_\Lambda}, \overline{p^*_\pi})| < 0.90$ cut.

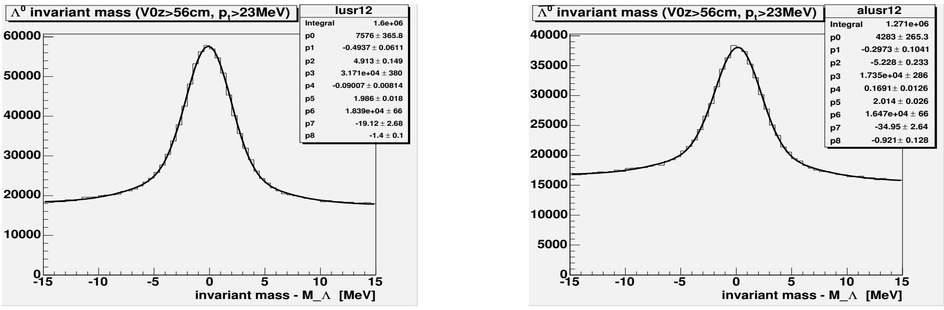

Figure 5.10: Λ^0 (left) and $\overline{\Lambda^0}$ (right) mass distributions ($z_{V^0} > 56$ cm, $p_t > 23$ MeV).

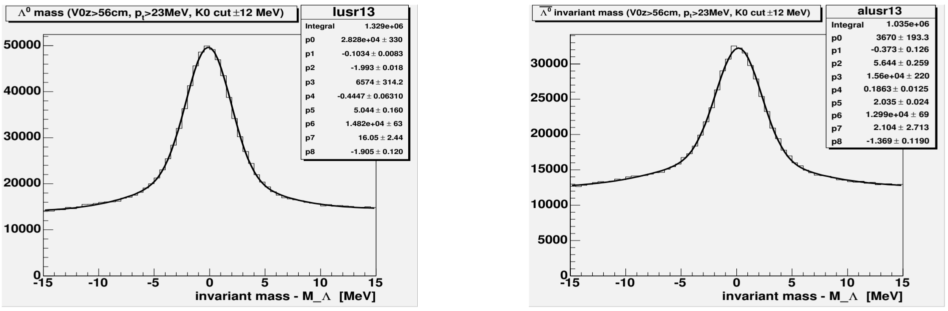

Figure 5.11: Λ^0 (left) $\overline{\Lambda^0}$ (right) mass distributions ($z_{V^0} > 56$ cm, $p_t > 23$ MeV, rejection of K^0 particles).

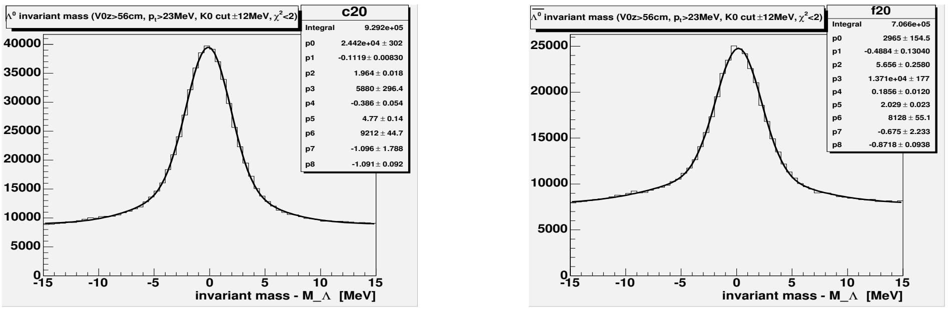

Figure 5.12: Λ^0 (left) and $\overline{\Lambda^0}$ (right) mass distribution ($z_{V^0} > 56$ cm, $p_t > 23$ MeV, rejection of K^0 particles, $\chi^2 < 2$).

	Λ^0		$\overline{\Lambda^0}$	
Cut	S	S/B	S	S/B
<0.95	353 029	1.33	199 578	0.86
<0.90	**339 206**	**1.45**	**193 340**	**0.96**
<0.85	324 119	1.55	186 849	1.04
<0.80	303 716	1.62	176 447	1.11

Table 5.8: The Λ^0, $\overline{\Lambda^0}$ signals and S/B ratios for different $|\cos(\overline{p^*_\Lambda}, \overline{p^*_\pi})|$ cuts ($z_{V^0} > 56$ cm, $p_t > 23$ MeV, K^0 ± 12 MeV cut, $\chi^2 < 2$ cuts). The cut in bold is used in the analysis.

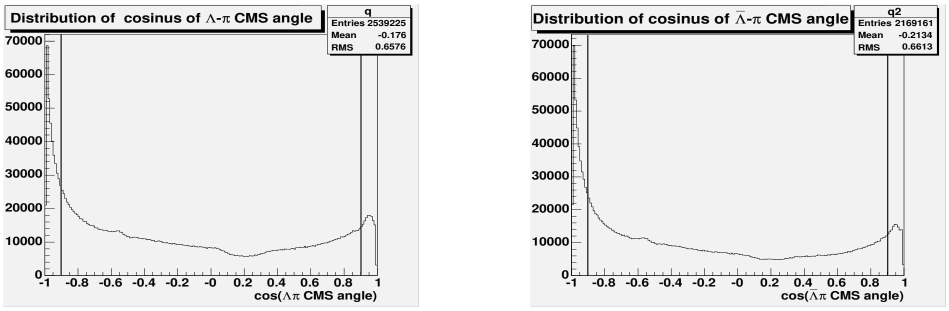

Figure 5.13: $\cos(\overline{p^*_\Lambda}, \overline{p^*_\pi})$ (left) and $\cos(\overline{p^*_{\overline{\Lambda}}}, \overline{p^*_\pi})$ (right) angle distributions.

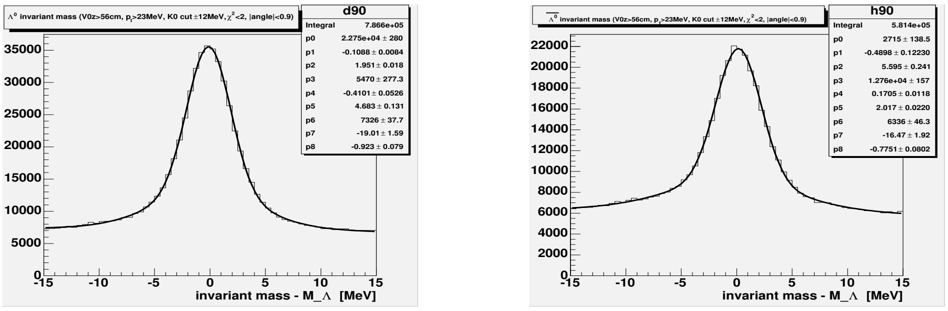

Figure 5.14: Λ^0 (left) and $\overline{\Lambda^0}$ (right) mass distributions ($z_{V^0} > 56$ cm, $p_t > 23$ MeV, K^0 ± 12 MeV cut, $\chi^2 < 2$, $|\cos(\overline{p^*_\Lambda}, \overline{p^*_\pi})| < 0.90$).

5.2.6 Cuts on RICH identification

The demand that one or both particles from a V^0 vertex were identified in the RICH detector is the criterion that should greatly improve signal-to-background ratio. After these cuts the significance of both peaks increases but the sample statistics drops down. In Figs 5.15–5.16 the Λ^0 and $\overline{\Lambda^0}$ mass distributions with RICH identification cuts are shown. Results of the cuts are summarized in Table 5.9. RICH identification of particles from Λ^0 and $\overline{\Lambda^0}$ decays will not be used in the pentaquark analysis.

	Λ^0		$\overline{\Lambda^0}$	
Cut	S	S/B	S	S/B
one particle identified	41 052	3.98	22 356	2.52
both particles identified	5 102	12.44	3 038	6.58

Table 5.9: The Λ^0, $\overline{\Lambda^0}$ signals and S/B ratios with a demand that one or both particles were identified in RICH ($z_{V^0} > 56$ cm, $p_t > 23$ MeV, K^0 ± 12 MeV cut, $\chi^2 < 2$, $|\cos(\overline{p^*_\Lambda}, \overline{p^*_\pi})| < 0.90$ cuts).

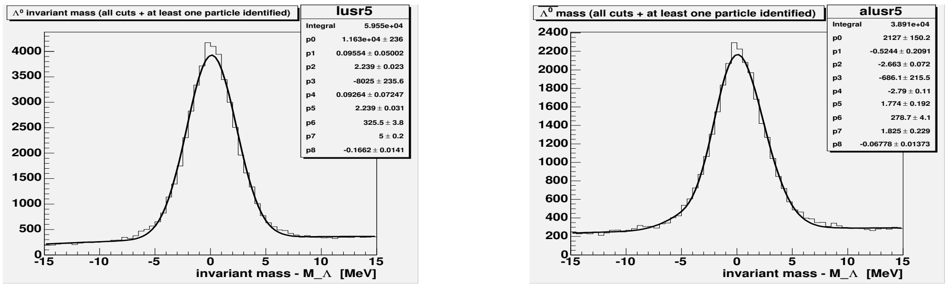

Figure 5.15: Λ^0 (left) and $\overline{\Lambda^0}$ (right) mass distributions with at least one particle identified ($z_{V^0} > 56$ cm, $p_t > 23$ MeV, K^0 ± 12 MeV cut, $\chi^2 < 2$, $|\cos(\overline{p^*_\Lambda}, \overline{p^*_\pi})| < 0.90$).

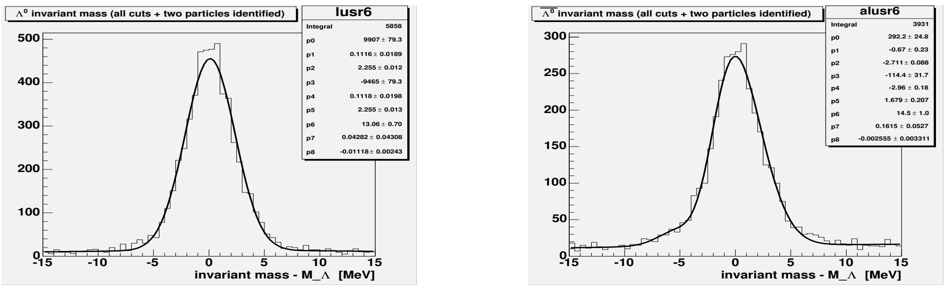

Figure 5.16: Λ^0 (left) and $\overline{\Lambda^0}$ (right) mass distributions with both particles identified ($z_{V^0} > 56$ cm, $p_t > 23$ MeV, K^0 ± 12 MeV cut, $\chi^2 < 2$, $|\cos(\overline{p^*_\Lambda}, \overline{p^*_\pi})| < 0.90$).

5.2.7 Discussion of the Λ^0 and $\overline{\Lambda^0}$ signals

The Λ^0 and $\overline{\Lambda^0}$ candidates defined with the cuts described in sections 5.2.1–5.2.5 ($z_{V^0} > 56$ cm, $p_t > 23$ MeV, rejection of K^0 admixture, $\chi^2 < 2$, $|\cos(\overline{p^*_\Lambda}, \overline{p^*_\pi})| < 0.90$) are kept for further analysis. The number of Λ^0 exceeds the number of $\overline{\Lambda^0}$ by a factor of 1.7–1.8 which may to certain extend reflect the initial asymmetry between baryons, and antibaryons. A sum of two Gaussian functions and a second degree polynomial is chosen to approximate the signals and the backgrounds respectively. The reason for choosing the sum of two Gaussian functions is the same as in the case of K^0 analysis (see Sec. 5.1.6). Tables 5.10 and 5.11 summarize the Λ^0 and $\overline{\Lambda^0}$ cuts.

Cut	S	Relative S [%]	S/B	Relative S/B
no cuts	920 022	100.0	0.05	1.0
$z_{V^0} > 56$ cm	480 017	52.2	0.54	10.8
$p_t > 23$ MeV	482 262	52.4	0.82	16.4
$m_{K^0} \pm 12$ MeV cut	429 436	46.7	0.91	18.2
$\chi^2 < 2$	367 537	39.9	1.25	25.0
$\|\cos(\overline{p^*_\Lambda}, \overline{p^*_\pi})\| < 0.90$	339 206	36.9	1.45	29.0

Table 5.10: Final cuts for the Λ^0 selection.

Cut	S	Relative S [%]	S/B	Relative S/B
no cuts	463 267	100.0	0.03	1.0
$z_{V^0} > 56$ cm	267 393	57.7	0.30	10.0
$p_t > 23$ MeV	272 813	58.9	0.52	17.3
$m_{K^0} \pm 12$ MeV cut	246 347	53.2	0.59	19.7
$\chi^2 < 2$	210 001	45.3	0.81	27.0
$\|\cos(\overline{p^*_{\overline{\Lambda}}}, \overline{p^*_\pi})\| < 0.90$	193 340	41.7	0.96	32.0

Table 5.11: Final cuts for the $\overline{\Lambda^0}$ selection.

Chapter 6

K^0 and Λ^0 yields in the Monte Carlo and in the COMPASS data

Comparison of the K^0 and Λ^0 yields measured in the COMPASS experiment with yields obtained from the Monte Carlo simulation is a crucial test of our understanding of the data analysis and of the spectrometer performance. There are two reasons why the comparison involves these two particles. First, their properties are very well known; second, they are produced copiously off the COMPASS target (see Sec. 5). This allows to make tests with a high data statistics. In such tests a systematic error, which is being checked, dominates the statistical error. These tests have to be made before a complicated analysis of possible signals from new particles such as pentaquarks.

6.1 Comparision of K^0 yields in the Monte Carlo and in the 2002 P2E period data

K^0 is the lightest strange meson. Its mass is equal to (497.672 ± 0.031) MeV. In COMPASS it is only possible to observe K^0_S particles while the K^0_L variety escapes the detector. K^0_S decays in most cases into $\pi^+\pi^-$ pairs (see also Sec. 3.1). This channel is used for comparison of data and Monte Carlo yields. Identical cuts are applied to both event samples.

6.1.1 The Monte Carlo sample

The Monte Carlo sample of 260 000 events was generated with PYTHIA 6.2 – the Lund Monte Carlo generator. Generated events were then passed through the COMGEANT (the COMPASS simulation program based on GEANT 3.21) and reconstructed with CORAL. The only kinematical cut applied at the PYTHIA generation level was $y > 0.07$. Events which did not satisfy this cut were rejected. About 2.1% of events failed an internal PYTHIA fragmentation cut; this number should be close to zero if the generator works correctly. Number of events that fail fragmentation cut depends on the y cut. An example of this dependence is presented in Table 6.1.

y_{min}	σ (μb)	fail fragm. cuts (%)
0.01	5.03	36.4
0.02	4.72	34.8
0.05	2.79	2.1
0.07	2.25	2.1
0.10	1.72	2.0
0.35	0.42	1.1

Table 6.1: Percentage of events that fail fragmentation cut for different y cuts. Cross section σ for μN interactions is also given.

The choice of $y_{min} = 0.07$ was made since it satisfies two general demands: the μN interaction cross section is still large (the cross section decreases with increasing y_{min}), and the percentage of the events that failed fragmentation cut is of the order of two percent which seems to be an acceptable value [24]. An integrated Monte Carlo luminosity can be calculated. With 260 000 generated events and a cross section of 0.00225 mb (see Table 6.1) it is equal to:

$$\mathcal{L}_{MC} = \frac{260000}{0.00225 \cdot 10^{-27}\text{cm}^2} = 0.116 \cdot 10^{36} \frac{1}{\text{cm}^2} \tag{6.1}$$

6.1.2 The Real Data sample

For the K^0 Real Data – Monte Carlo comparison data from P2E period were chosen. The P2E period consists of more than 200 physics runs out of which two were taken for the analysis – runs 22414 and 22448. Together they contain 1 884 724 events. The incident muon flux for run 22414 is equal $2.047{\cdot}10^{10}$ and for run 22448 it is $2.003{\cdot}10^{10}$. The total flux for both runs is equal $4.050{\cdot}10^{10}$. Fluxes were calculated using a purpose written PHAST procedure.

To calculate the luminosity a number of scattering centres in the target per 1 cm^2 is needed. It is given by:

$$C = \frac{N_A}{V} l \sum_{k=1}^{10} A_k P_k = 3.488 \cdot 10^{25} \frac{1}{\text{cm}^2} \tag{6.2}$$

where N_A is the Avogadro number, V is the target volume, l is the target length, A_k is the atomic mass of the k element and P_k is the number of mols of this element in the target (see Table 2.1). Luminosity is a product of a flux and a surface density of scattering centers. It is thus equal to $\mathcal{L}_{RD} = 1.413 \cdot 10^{36}\text{cm}^{-2}$.

6.1.3 Selection of K^0 events

Cuts leading to the best K^0 signal were described in Sec. 5.1. In the Monte Carlo and Real Data comparison those criteria are different:

- A primary vertex is inside the target in z-axis, *i.e.* $z > -100$ cm and $z < -40$ cm or $z > -30$ cm and $z < 30$ cm.
- A V^0 vertex is situated outside the target, *i.e.* $(z_{V^0}) > 56$ cm (see Sec. 5.1).
- The invariant mass of the system of two particles forming the V^0 is in the range of nominal K^0 mass ± 25 MeV (assuming both outgoing particles are pions).

Two additional cuts are applied:

- A primary vertex contains an incoming and a scattered muon so that the y variable can be calculated and a cut $y > 0.07$ is applied.
- Events with inelasticity[1] smaller than 2.5 GeV and with three particles outgoing from the primary vertex are rejected.

First of these cuts is obvious because the same cut is applied on the Monte Carlo sample. The second cut removes diffractive production which does not exist in the Monte Carlo generator. Events with more than one primary vertex are not rejected and it is assumed that the 'real' primary vertex is the one with the best χ^2.

Using the above criteria a selection of K^0 in both samples is performed.

[1] For the definition of inelasticity see [21]

6.1.4 Results

Number of K^0 candidates found in the Monte Carlo and in the Real Data is N_{MC} =985 and N_{RD} =3 848. Before comparing these numbers a normalization of both samples to the same luminosity has to be done. This means that the number of K^0 in Monte Carlo should be multiplied by a ratio of $\mathcal{L}_{RD}$ over $\mathcal{L}_{MC}$ in order to obtain the expected number of K^0 mesons.

$$N_{expected} = N_{MC}\frac{\mathcal{L}_{RD}}{\mathcal{L}_{MC}} = 12041 \tag{6.3}$$

The ratio of the expected (from the Monte Carlo simulation) yield of the K^0 candidates to this measured in the COMPASS experiment is thus equal to:

$$\left(\frac{N_{expected}}{N_{RD}}\right)_{K^0} = \left(\frac{12041}{3848}\right) = 3.13 \tag{6.4}$$

6.2 Comparison of Λ^0 yields in the Monte Carlo and in the 2002 P2D period data

The Λ^0 particle is the lightest strange baryon. Its mass is equal to (1115.683 ± 0.006) MeV. The main decay channel for this particle is $\Lambda^0 \rightarrow p\pi^-$ (see also Sec. 3.1). Identical cuts are applied in the Monte Carlo and the Real Data samples which are used in the comparison.

6.2.1 The Monte Carlo sample

The Monte Carlo sample was generated with PYTHIA 6.2. Then, just like in the K^0 case, the generated events were passed through COMGEANT and reconstructed with CORAL. Kinematical cut $y > 0.07$ was applied in PYTHIA. Moreover 56% of events that did not satisfy triggers conditions were rejected. Finally 480 984 generated events were retained. The integrated Monte Carlo luminosity for a cross section of 0.00225 mb is thus equal to:

$$\mathcal{L}_{MC} = \frac{480984}{0.44 \cdot 0.00225 \cdot 10^{-27}\mathrm{cm}^2} = 4.858 \cdot 10^{36}\frac{1}{\mathrm{cm}^2} \tag{6.5}$$

6.2.2 The Real Data sample

Data from 70 runs taken at the beginning of the P2D period are taken. Two built-in PHAST methods are used to estimate the incident muon flux. The first one, the 'spill-time range' method, give a result of $112.868 \cdot 10^{10}$. The second method – 'event-event time' – give the result of $112.115 \cdot 10^{10}$. These results are consistent at the level of 0.5%. As the expected difference between Monte Carlo and Real Data is at the level of 300% the above difference is negligible and both flux values can be used in the analysis. The first value is chosen. The Real Data luminosity is a product of a flux and a surface density of scattering centres calculated in Sec. 6.1.2 and is equal to $\mathcal{L}_{RD} = 39.368 \cdot 10^{36}\text{cm}^{-2}$.

6.2.3 Selection of Λ^0 events

The comparison of Monte Carlo sample with Real Data concerns the Λ^0 produced in the primary interaction. The cuts are similar to those in Sec. 5.2:

- An event should contain only one primary vertex.
- A primary vertex is inside the target in z-axis, *i.e.* $z > -100$ cm and $z < -40$ cm or $z > -30$ cm and $z < 30$ cm.
- A primary vertex is inside a target in thy (x,y) plane, *i.e.* $r < 1.5$ cm, where $r = \sqrt{x^2 + y^2}$.
- V^0 vertices with $\chi^2 > 2$ are rejected.
- The angular difference between the momentum vector of the $p\pi$ system and the straight line connecting the primary and lambda decay vertices should be smaller than 0.01 radians (this cut chooses Λ^0 outgoing from the primary interaction point).
- z of the Λ^0 decay vertex should be greater than 56 cm, *i.e.* the decay vertex is outside the target vessel.
- $y > 0.1$ and $y < 0.9$. Those cuts are introduced following [23].
- V^0 vertices with outgoing particles having $p_t < 23$ MeV are rejected.

Using the above criteria a selection of Λ^0 in both samples is performed. The PHAST 6.004 program is used.

6.2.4 Results

Number of Λ^0 candidates found in the Monte Carlo and in the Real Data is N_{MC} =6 732 and N_{RD} =15 166. Before comparing these numbers a normalization of both samples to the same luminosity has to be done. This means that the number of Λ^0 in Monte Carlo should be multiplied by a ratio of $\mathcal{L}_{RD}$ over $\mathcal{L}_{MC}$ in order to obtain the expected number of Λ^0 hyperons.

$$N_{expected} = N_{MC}\frac{\mathcal{L}_{RD}}{\mathcal{L}_{MC}} = 54550 \tag{6.6}$$

Finally the ratio of the expected (Monte Carlo simulation) yield of the Λ^0 candidates to this measured in the experiment can be derived:

$$\left(\frac{N_{expected}}{N_{RD}}\right)_{\Lambda^0} = \left(\frac{54550}{15166}\right) = 3.60 \tag{6.7}$$

6.3 Summary

It was found that the ratios of the K^0 meson and Λ^0 baryon yields in the data and in the Monte Carlo are similar – between 3 and 4. It is in a good agreement with the ratios calculated for the D^0 and D^* mesons [25]. This severe discrepancy between the Monte Carlo and the Real Data is not yet fully understood.

Chapter 7

The Θ^+ pentaquark analysis

The invariant mass systems in which Θ^+ and $\overline{\Theta^+}$ pentaquarks should be visible can be studied in the COMPASS detector *via* the following decays:

$$\Theta^+ \to pK^0 \to pK_s^0 \to p\pi^+\pi^- \tag{7.1}$$

$$\overline{\Theta^+} \to \overline{p}\overline{K^0} \to \overline{p}K_s^0 \to \overline{p}\pi^+\pi^- \tag{7.2}$$

The K_s^0 (denoted in the analysis as K^0) sample selected for this search is defined with the cuts described in Sec. 5.1 (the cut on RICH identification is not used). Only the candidates with an invariant mass in the nominal K^0 mass ± 12 MeV interval are retained. The final sample contains 1 658 057 K^0 candidates with S/B ratio of 13.06. The K^0 mesons are paired with the particles of the appropriate charge (positive in case of Θ^+ and negative in case of $\overline{\Theta^+}$) outgoing from the primary vertex. The studies are divided into two parts. In the first part the particles from primary vertices do not have to be identified in RICH as protons. In the second part the RICH identification of protons is required.

7.1 Studies without proton identification

7.1.1 Motivation

The momentum threshold for protons identification in RICH is about 17 GeV. Most of the protons originating from the decays of the particles with masses close to the phase space limits (like $\Lambda^0(1520)$ or Θ^+) have momenta below that threshold. Therefore studies without proton identification in RICH are performed. However in this case the sample contains many pK^0 pairs with fake protons, that in fact are pions or kaons. This strong background may conceal the pentaquark signal. In Fig. 7.1 invariant mass spectra of pK^0 and $\overline{p}K^0$

systems are presented. A sum for both channels is also plotted. An arrow indicates the mass where the expected pentaquark peak should be located. The distributions of invariant masses do not reveal any structures in the 1500–1580 MeV mass range.

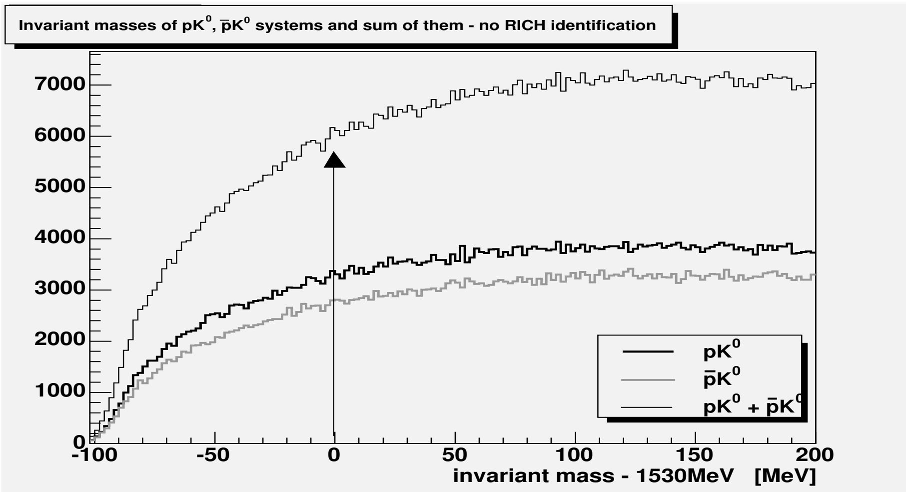

Figure 7.1: pK^0 and $\overline{p}K^0$ invariant masses (no RICH identification).

7.1.2 Proton candidates with momenta greater than 2.5 GeV

Protons can be identified if their energy exceeds 17 GeV. Threshold for pion identification is much lower: about 2.5 GeV. Over 90% of particles outgoing from primary vertices are pions. Therefore it is obvious that the background in the pentaquark analysis is mainly due to pions treated as if they were protons. To reduce this background a demand that a proton candidate momentum exceeds 2.5 GeV and it is not identified as a pion (or a kaon) is used. The proton identification in RICH is still not required. The invariant masses with the above cut are presented in Fig. 7.2. No peak in the pentaquark mass range is visible after this cut.

7.1.3 Removing the $K^*(892)$ mesons

In Figs. 4.20 and 4.23, $K^{*0}(892)$ and $\overline{K^{*0}}(892)$ mass distributions were plotted. Besides the chargeless $K^*(892)$ states two charged states of this particle exist: $K^{*-}(892)$, $K^{*+}(892)$. Their decay channels are:

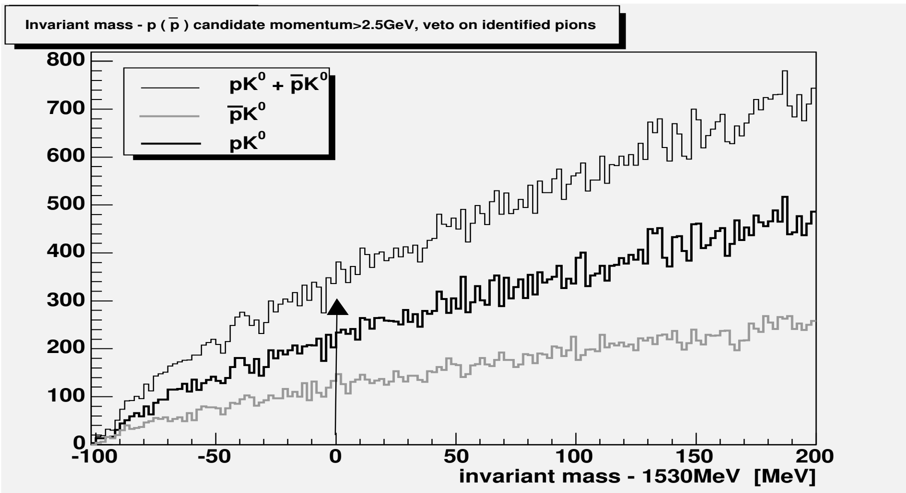

Figure 7.2: pK^0 and $\overline{p}K^0$ invariant masses (proton candidate momentum> 2.5 GeV, identified π and K rejected).

$$K^{*-}(892) \rightarrow \pi^- K^0 \tag{7.3}$$

$$K^{*+}(892) \rightarrow \pi^+ K^0 \tag{7.4}$$

These particles decay practically in the primary vertices. In Figs. 7.3 and 7.4 invariant masses of $\pi^- K^0$ and $\pi^+ K^0$ systems reveal both states. The plots are made with a demand that π mesons are identified in the RICH. To reject the K^0 particles emerging from $K^{*-}(892)$ or $K^{*+}(892)$ decays the following procedure is used. Each K^0 candidate is paired with each particle outgoing from the primary vertex. The particle is assumed to be a pion. If the invariant mass of that system is in the range of 850–930 MeV, a K^0 is rejected since it is probable that it originates from a $K^{*+}(892)$ or $K^{*-}(892)$ decay. No Θ^+ or $\overline{\Theta^+}$ peaks emerge after these cuts (Fig. 7.5).

7.1.4 Low momenta K^0

As a simplified Monte Carlo simulation [26] predicts, momenta of K^0 mesons from the Θ^+ decays very rarely exceed 9 GeV. Therefore a cut removing K^0 with high momenta rejects only the particles that are produced directly in a primary interaction or originate from decays of other particles having a wider allowed phase space for their decay products. Three different cuts on a maximal

K^0 momentum are tried: 12 GeV, 9 GeV, 6 GeV. Obtained invariant mass plots do not reveal any structures inconsistent with the background (see Fig. 7.6).

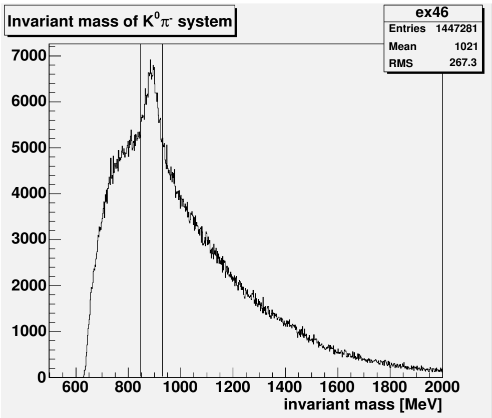

Figure 7.3: $\pi^- K^0$ invariant mass distribution and the $K^{*-}(892)$ signal.

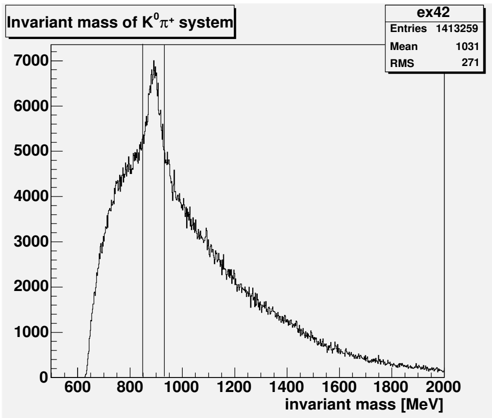

Figure 7.4: $\pi^+ K^0$ invariant mass distribution and the $K^{*+}(892)$ signal.

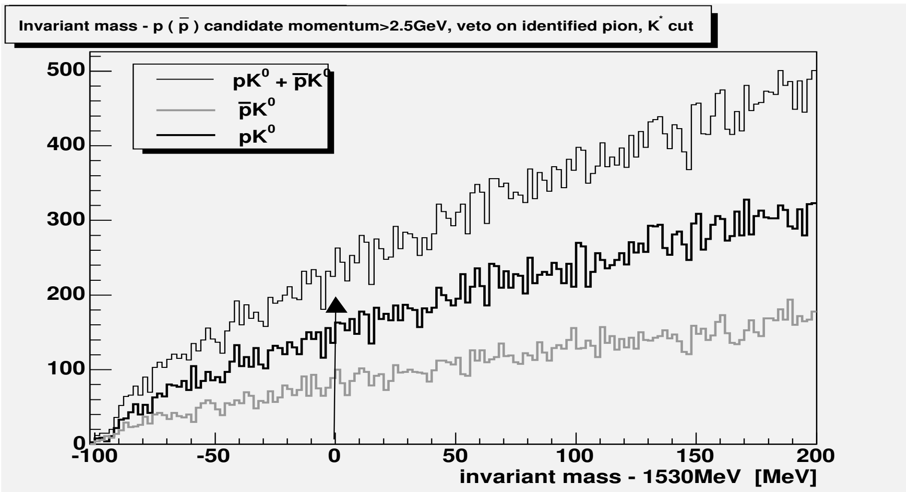

Figure 7.5: pK^0 and $\overline{p}K^0$ invariant masses (proton candidate momentum> 2.5 GeV, identified π and K rejected, $K^*(892)$ cut).

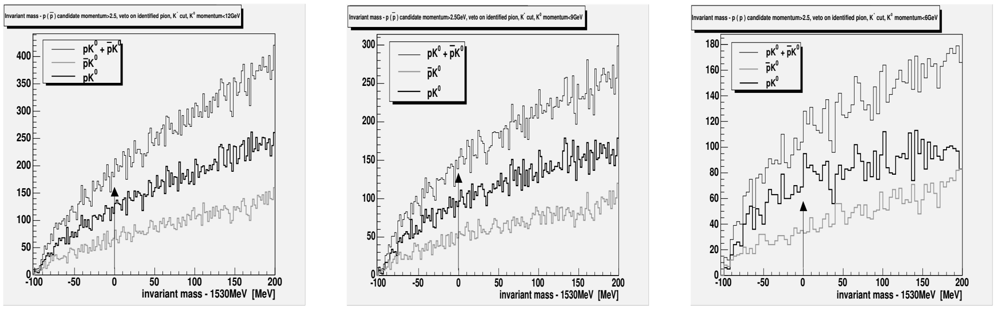

Figure 7.6: pK^0 and $\overline{p}K^0$ invariant masses for different K^0 momentum cuts: 12 GeV, 9 GeV, 6 GeV (proton candidate momentum> 2.5 GeV, identified π and K rejected, $K^*(892)$ cut).

7.1.5 Cut on x_F

Production of the Θ^+ should most probable occur in the target fragmentation region, that is at low values of the Feynman variable x_F [27]. Different cuts on x_F are tried. None of them results in a peak in the 1500–1580 MeV mass range. In Fig. 7.7 invariant masses with cut on $x_F < 0.35$ are presented.

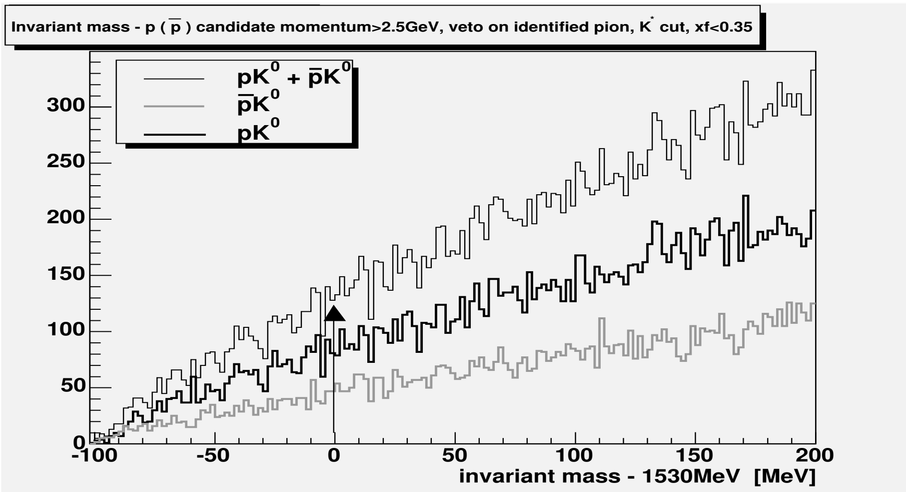

Figure 7.7: pK^0 and $\overline{p}K^0$ invariant masses (proton candidate momentum> 2.5 GeV, identified π and K rejected, $K^*(892)$ cut, $x_F < 0.35$).

7.1.6 Cut on the vertex position

Finally a cut on z coordinate of a primary vertex is applied. Particles that are produced in the target interact electromagnetically within its dense material. The interactions may cause perturbations in the particles' trajectory that would preclude good reconstruction of a narrow Θ^+ state. Therefore a demand that a primary vertex has to be inside the second half of the downstream target cell ($z > 0$ cm) should help in revealing the pentaquark peak. The invariant masses with that demand are presented in Fig. 7.8. No peak is visible.

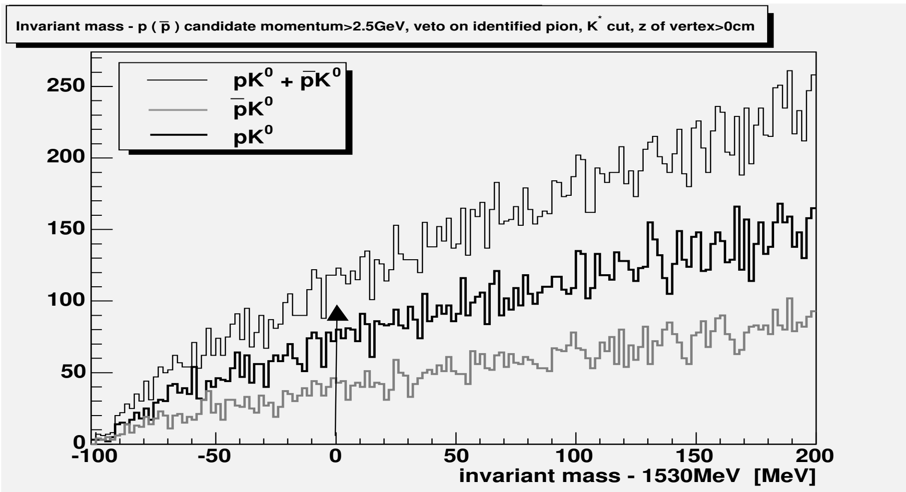

Figure 7.8: pK^0 and $\overline{p}K^0$ invariant masses (proton candidate momentum> 2.5 GeV, identified π and K rejected, $K^*(892)$ cut, $z > 0$ cm).

7.1.7 All cuts

In Fig. 7.9 invariant masses of pK^0 and $\overline{p}K^0$ with all the cuts described above are presented. These cuts are: proton candidate momentum greater than 2.5 GeV, proton candidates identified as π or K rejected, K^0 from $K^*(892)$ decays rejected, K^0 momentum smaller than 6 GeV, $x_F < 0.35$, $z > 0$ cm. No Θ^+ or $\overline{\Theta^+}$ peaks emerge after imposing all the cuts. A small excess of events around the 1540 MeV mass is consistent with the background.

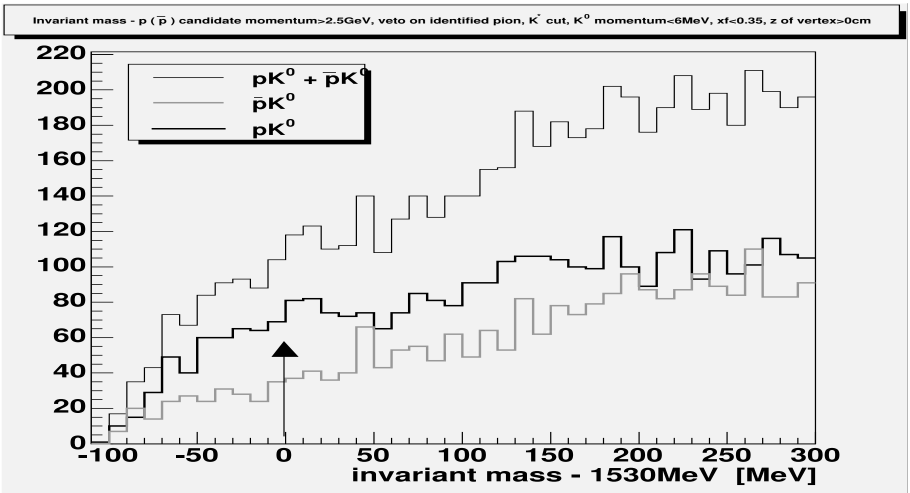

Figure 7.9: pK^0 and $\overline{p}K^0$ invariant masses (proton momentum$>$ 2.5 GeV, identified π and K rejected, $K^*(892)$ cut, K^0 momentum$<$ 6 GeV, $x_F < 0.35$, $z > 0$ cm).

7.2 Θ^+ studies with RICH identification

7.2.1 Motivation

The allowed phase space for Θ^+ decay is similar to the phase space for $\Lambda^0(1520)$ decay. If the cross section for the Θ^+ production is comparable or larger than that for the $\Lambda^0(1520)$ (as the HERMES Collaboration suggests [9]), the studies with RICH identification could reveal the pentaquark peak. The $\Lambda^0(1520)$ production signal is questionable (see Sec. 4.4.3) but the reconstruction of Θ^+ may be easier. A difference between both analyses is that in case of the $\Lambda^0(1520)$ both decay products have to be identified in the RICH while in case of Θ^+ only a proton needs identification. The K^0 sample is already clean due to cuts described in Sec. 5.1. The $\Lambda^0(1520)$ phase space is thus reduced by the two RICH cuts while the Θ^+ phase space only by one. Unfortunately distributions of invariant pK^0 and $\overline{p}K^0$ masses do not reveal any peaks which could be associated with Θ^+ or $\overline{\Theta^+}$ pentaquarks (Fig. 7.10).

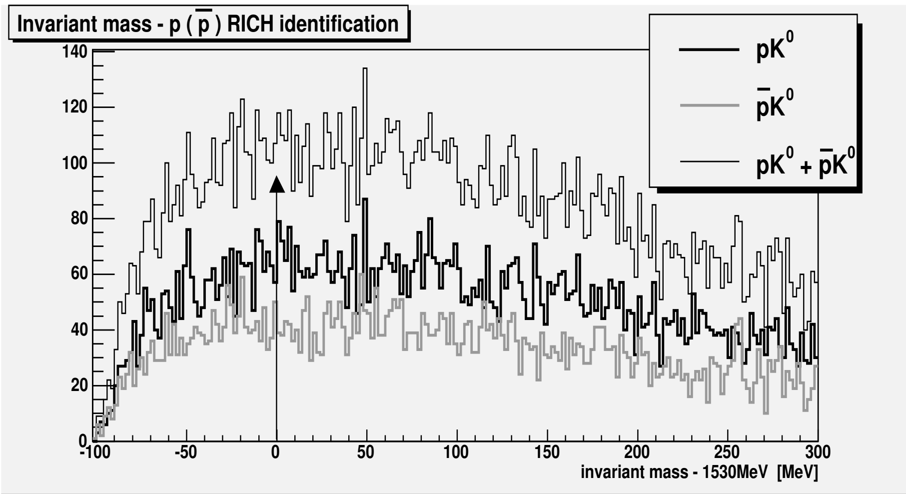

Figure 7.10: pK^0 and $\overline{p}K^0$ invariant masses (p and $\overline{p}$ RICH identified).

7.2.2 Cuts on $K^*(892)$, z and K^0 momentum

Additional studies similar to those from the no-RICH case are performed (see Sec. 7.1). The following cuts are imposed:

- Cut on $K^*(892)$ and $\overline{K^*}(892)$ particles (see Fig. 7.11).
- Cut on $z > 0$ cm (see Fig. 7.12).
- Three different cuts on maximal K^0 momentum: 9 GeV, 12 GeV, 15 GeV (see Fig. 7.13).

The cuts do not reveal any pentaquark signal. A small excess of the events with an invariant mass equal to about 1560 MeV can be observed in Fig. 7.13, most probably due to the statistical fluctuations of the background.

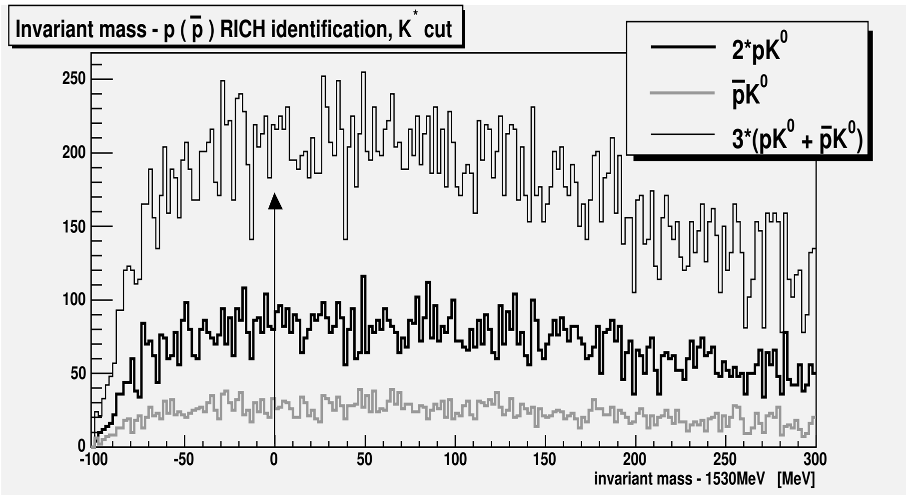

Figure 7.11: pK^0 and $\overline{p}K^0$ invariant masses (p and $\overline{p}$ RICH identified, $K^*(892)$ cut). The plot for pK^0 is multiplied by 2, the plot presenting the sum of both channels is multiplied by 3.

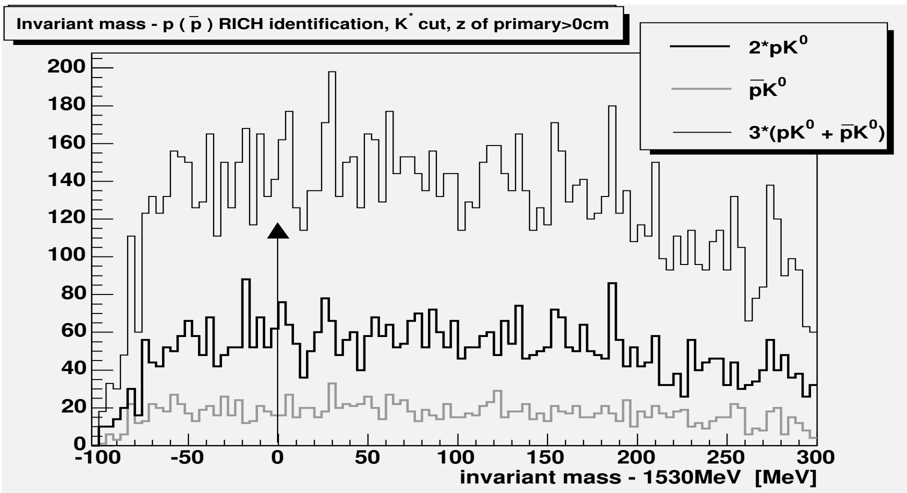

Figure 7.12: pK^0 and $\overline{p}K^0$ invariant masses (p and $\overline{p}$ RICH identified, $K^*(892)$ cut, $z > 0$ cm). The plot for pK^0 is multiplied by 2, the plot presenting the sum of both channels is multiplied by 3.

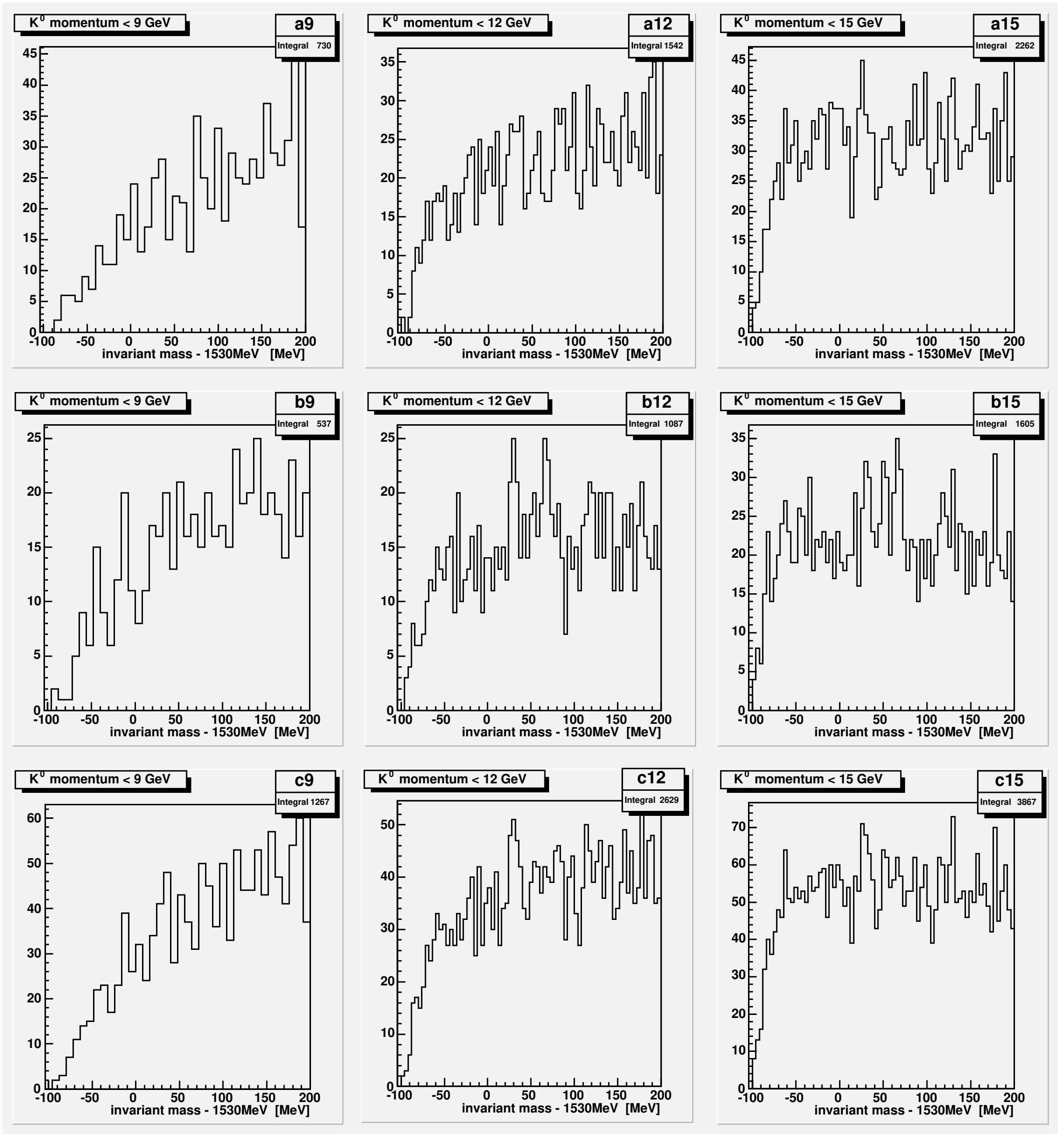

Figure 7.13: pK^0 and $\overline{p}K^0$ invariant masses (p and $\overline{p}$ RICH identified, $K^*(892)$ cut). In columns – different cuts on a maximal K^0 momentum (9 GeV, 12 GeV, 15 GeV), in rows – pK^0, $\overline{p}K^0$, $pK^0 + \overline{p}K^0$ mass distributions.

Chapter 8

Ξ^- and $\Xi^0(1530)$ states

8.1 Ξ^- and $\overline{\Xi^-}$ samples

Ξ^- ($\overline{\Xi^-}$) decays into a $\pi^-\Lambda^0$ ($\pi^+\overline{\Lambda^0}$) pair. The reconstruction of Ξ^- ($\overline{\Xi^-}$) states is performed by pairing Λ^0 ($\overline{\Lambda^0}$) candidates (defined in Sec. 5.2) with pion candidates of appropriate charge. To obtain the Ξ^- and $\overline{\Xi^-}$ signals the following cuts are applied:

- The Λ^0 and $\overline{\Lambda^0}$ samples are defined with the cuts described in Sec. 5.2 (cut on RICH identification is not used). Moreover all Λ^0 ($\overline{\Lambda^0}$) candidates that have an invariant mass outside the nominal Λ^0 ± 5 MeV interval are discarded. The final samples contain 312 123 Λ^0 and 175 388 $\overline{\Lambda^0}$ candidates with S/B ratios of 2.13 and 1.39 respectively.

- A pion candidate is a particle with an appropriate charge, negative for Ξ^- studies and positive for $\overline{\Xi^-}$ studies.

- A pion candidate is rejected if a primary vertex is among vertices the pion can be associated with (a set of such vertices is created by CORAL during reconstruction process).

- The closest distance between Λ^0 ($\overline{\Lambda^0}$) track (a straight line) and a pion candidate track (propagated through a magnetic field with a PHAST *FindCDA* procedure) has to be smaller than 1 mm. The point on a pion candidate track at z corresponding to the shortest distance is called Ξ^- ($\overline{\Xi^-}$) vertex.

- $z_\Xi > z_{primary}$.

- $z_\Lambda > z_\Xi$.

First two cuts are denoted as minimal cuts. The cuts are discussed in the following sections. Signals and signal-to-background ratios are calculated in the ± 15 MeV mass windows centred at the Ξ^- PDG mass. The signal peaks and the background are fitted with a sum of a Gaussian and a second degree polynomial.

8.1.1 Cut on a pion vertex

Particles registered in the COMPASS detector originate from a primary or secondary vertex. A CORAL reconstruction program ascribes tracks to appropriate vertices. This procedure is often not unique. Therefore a particle track may be ascribed to a few vertices one of which can be a primary one. The lifetime of Ξ^- ($\overline{\Xi^-}$) is long enough for this particle to decay far from the primary interaction point. Therefore a pion originating from such a decay should not be attributed to a primary vertex. After rejecting pions attributed to primary vertices 5219 (S/B=0.39) Ξ^- and 3288 (S/B=0.37) $\overline{\Xi^-}$ candidates are left. Without this cut the corresponding numbers are 5452 (S/B=0.11) Ξ^- and 3418 (S/B=0.10) $\overline{\Xi^-}$. The invariant masses of Ξ^- and $\overline{\Xi^-}$ are presented in Fig. 8.1 – without pion vertex cut and in Fig. 8.2 – with the cut.

8.1.2 Cut on the closest distance between π and Λ^0 tracks

If Λ^0 ($\overline{\Lambda^0}$) and π originate from a Ξ^- ($\overline{\Xi^-}$) decay the tracks of both particles – Λ^0 ($\overline{\Lambda^0}$) and π – should have one common point in space. Due to an inaccuracy of measurement and reconstruction, tracks do not intersect. To find out if the tracks are correlated and originate from the same decay, the closest distance between them is calculated. The cut on that variable should improve signal-to-background ratio significantly. In Table 8.1 the results of different cuts on the closest distance are collected. In Fig. 8.3 the Ξ^- and $\overline{\Xi^-}$ signals with a demand that the distance is smaller than 1 mm are presented.

8.1.3 Cut on a primary – Ξ^- vertices distance

The production of the Ξ^- ($\overline{\Xi^-}$) particles occurs in a primary vertex. It is very unlikely that in the laboratory frame these particles go the upstream direction. Therefore events with Ξ^- ($\overline{\Xi^-}$) vertex located upstream the primary one should be considered as a background and removed from the sample. After this cut 3157 Ξ^- and 1911 $\overline{\Xi^-}$ particles remain. The signal-to-background ratios are 2.09 and 1.83, respectively. The invariant mass distributions are plotted in Fig. 8.4.

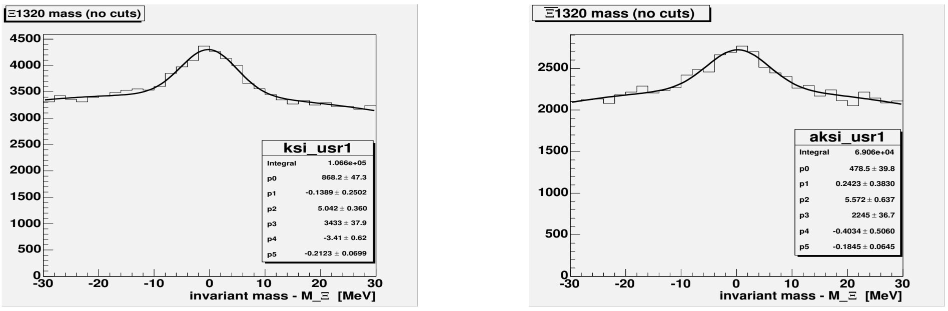

Figure 8.1: Ξ^- (left) and $\overline{\Xi^-}$ (right) mass distributions (minimal cuts).

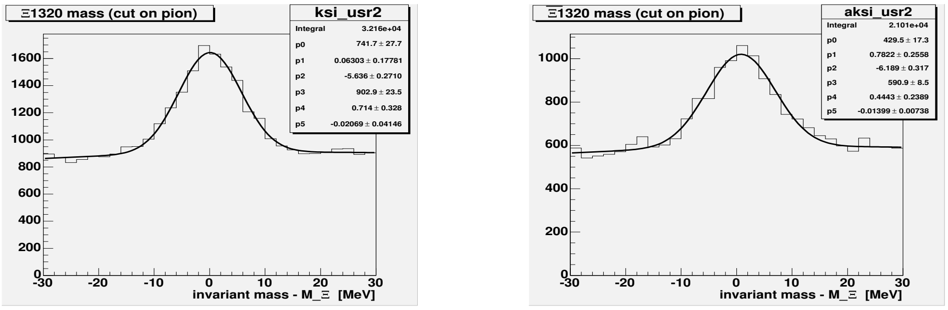

Figure 8.2: Ξ^- (left) and $\overline{\Xi^-}$ (right) mass distributions (pion vertex cut).

8.1.4 Cut on Ξ^-– Λ^0 vertices distance

If a Λ^0 particle is produced in a Ξ^- decay, Λ^0 decay vertex should be located downstream the Ξ^- decay vertex. The opposite order is improbable. The cut on the 'right' order of vertices should reduce the background. This cut retains 3126 (S/B=2.51) Ξ^- and 1883 (S/B=2.27) $\overline{\Xi^-}$ particles. In Fig. 8.5 the mass distributions for both states are plotted.

8.1.5 Cuts on RICH

Identification of particles in the RICH should significantly improve signal-to-background ratio but at the expense of a substantial decrease of statistics. In case of Ξ^- (or $\overline{\Xi^-}$) analysis three particles can be identified: a pion from a Ξ^- ($\overline{\Xi^-}$) decay, and a pion–proton pair from a Λ^0 ($\overline{\Lambda^0}$) decay. In Table 8.2 signals and S/B ratios for three different RICH cuts are presented. The cuts are: at least one particle from the Λ^0 ($\overline{\Lambda^0}$) decay is identified, both particles from the Λ^0 ($\overline{\Lambda^0}$) decay are identified, both particles from the Λ^0 ($\overline{\Lambda^0}$) decay plus a pion from the Ξ^- ($\overline{\Xi^-}$) decay are identified. A very small number of events remaining after those two last cuts makes it impossible to calculate meaningful the signal-to-background ratios.

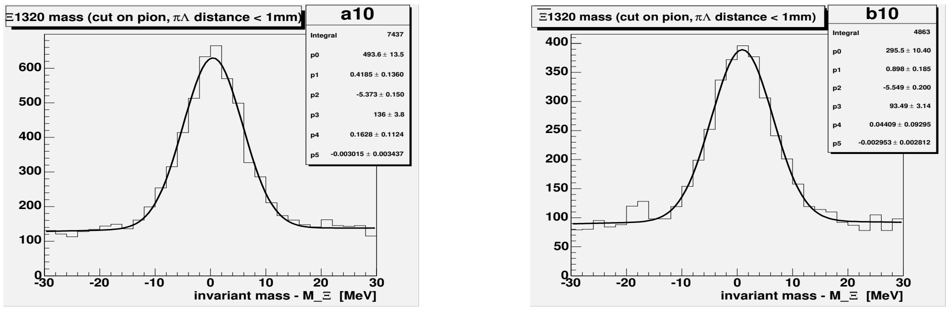

Figure 8.3: Ξ^- (left) and $\overline{\Xi^-}$ (right) mass distributions (pion vertex cut, π–Λ distance < 1 mm).

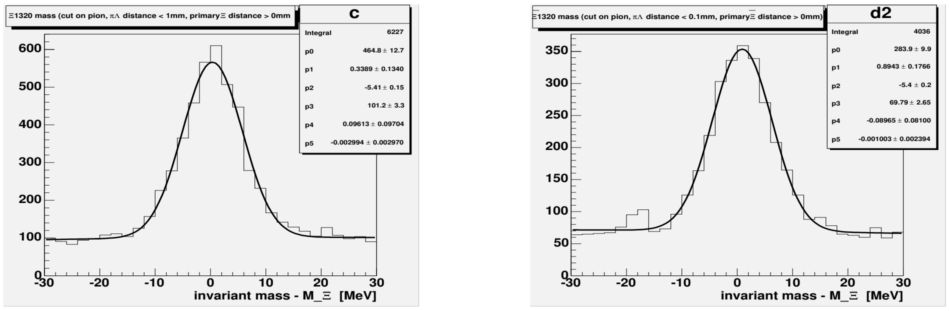

Figure 8.4: Ξ^- (left) and $\overline{\Xi^-}$ (right) mass distributions (pion vertex cut, π–Λ distance < 1 mm, primary–Ξ distance > 0 mm).

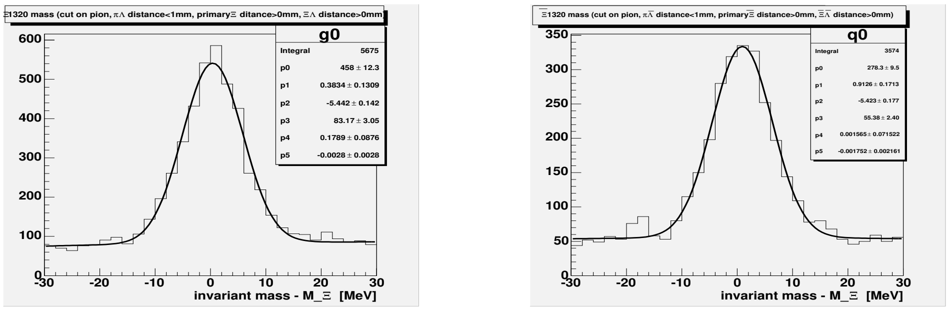

Figure 8.5: Ξ^- (left) and $\overline{\Xi^-}$ (right) mass distributions (pion vertex cut, π–Λ distance < 1 mm, primary–Ξ distance > 0 mm, Ξ–Λ distance > 0 mm).

	Ξ^-		$\overline{\Xi^-}$	
Cut [mm]	S	S/B	S	S/B
20	5216	0.47	3189	0.43
10	5060	0.58	3129	0.53
5	4904	0.81	2962	0.70
2	4340	1.30	2619	1.12
1	**3328**	**1.63**	**2041**	**1.46**
0.5	2263	1.95	1379	1.66

Table 8.1: The Ξ^-, $\overline{\Xi^-}$ signals and S/B ratios for different cuts on the closest distance between π and Λ tracks (cuts on: pion vertex). The cut in bold is used in the analysis.

	Ξ^-		$\overline{\Xi^-}$	
Cut	S	S/B	S	S/B
π^-_Λ (π^+_Λ) or p_Λ ($\overline{p_\Lambda}$)	427	3.85	272	5.44
π^-_Λ (π^+_Λ) and p_Λ ($\overline{p_\Lambda}$)	40	-	22	-
π^-_Λ (π^+_Λ) and p_Λ ($\overline{p_\Lambda}$) and π^-_Ξ (π^+_Ξ)	18	-	8	-

Table 8.2: The Ξ^-, $\overline{\Xi^-}$ signals and S/B ratios for different RICH cuts (other cuts: pion vertex, π–Λ distance < 1 mm, primary–Ξ distance > 0 mm, Ξ–Λ distance > 0 mm).

8.1.6 Discussion of Ξ^- and $\overline{\Xi^-}$ signals

Clear peaks of both Ξ^- and $\overline{\Xi^-}$ are obtained, Fig. 8.5. To all plots sums of a Gaussian and a second degree polynomial are fitted. All fits are satisfactory. Tables 8.3 and 8.4 summarize the effect of the cuts on the Ξ^- and $\overline{\Xi^-}$ signals (S) and on the signal-to-background (S/B) ratios. Numbers of particles obtained after all cuts (except the RICH cut) is 2–3 times higher than in NA49 analysis [13]. In NA49 1640 Ξ^- and 551 $\overline{\Xi^-}$ were found while in the 2002 COMPASS data the numbers are 3126 and 1883. The S/B ratios in both experiments are similar.

Cut	S	Relative S [%]	S/B	relative S/B
minimal cuts	5452	100.0	0.11	1.0
π not from a primary	5219	95.7	0.39	3.5
$\pi^- - \Lambda^0$ closest distance	3328	61.0	1.63	14.8
$z_\Xi > z_{primary}$	3157	57.9	2.09	19.0
$z_\Lambda > z_\Xi$	3126	57.3	2.51	22.8

Table 8.3: Final cuts for the Ξ^- selection.

Cut	S	Relative S [%]	S/B	relative S/B
minimal cuts	3418	100.0	0.10	1.0
π not from a primary	3288	96.2	0.37	3.7
$\pi^+ - \overline{\Lambda^0}$ closest distance	2041	59.7	1.46	14.6
$z_{\overline{\Xi}} > z_{primary}$	1911	55.9	1.83	18.3
$z_{\overline{\Lambda}} > z_{\overline{\Xi}}$	1883	55.1	2.27	22.7

Table 8.4: Final cuts for the $\overline{\Xi^-}$ selection.

8.2 Analysis of the $\Xi^0(1530)$ and $\overline{\Xi^0}(1530)$

8.2.1 $\Xi^0(1530)$ and $\overline{\Xi^0}(1530)$ invariant mass distributions

$\Xi^0(1530)$ and $\overline{\Xi^0}(1530)$ states are the only very well known particles (four stars significance in the PDG) decaying in the same channels as the hypothetical $\Xi^0_{3/2}$ and $\overline{\Xi^0_{3/2}}$ pentaquark states:

$$\Xi^0(1530) \to \Xi^-\pi^+ \to \Lambda^0\pi^-\pi^+ \to p\pi^-\pi^-\pi^+ \tag{8.1}$$

$$\overline{\Xi^0}(1530) \to \overline{\Xi^-}\pi^- \to \overline{\Lambda^0}\pi^+\pi^- \to \overline{p}\pi^+\pi^+\pi^- \tag{8.2}$$

Two minimal cuts are imposed to obtain $\Xi^0(1530)$ and $\overline{\Xi^0}(1530)$ signals:

- The Ξ^- and $\overline{\Xi^-}$ samples are defined with the cuts described in Sec. 8.1. Identification of particles in RICH is not used. The Ξ^- ($\overline{\Xi^-}$) candidates that have an invariant mass outside the ± 10 MeV window around the PDG value are discarded. The final numbers of Ξ^- and $\overline{\Xi^-}$ are 2921 and 1764 with signal-to-background ratios 3.52 and 3.19 respectively.

- A pion candidate is a particle with an appropriate charge (negative for $\Xi^0(1530)$ studies and positive for $\overline{\Xi^0}(1530)$) outgoing from a primary vertex.

A sum of a Gaussian and a second degree polynomial functions is fitted in the range of 1480–1750 MeV to the obtained $\Xi^0(1530)$ and $\overline{\Xi^0}(1530)$ peaks. The Ξ^0 and $\overline{\Xi^0}$ distributions are shown in Fig. 8.6. Their characteristics are collected in Table 8.5. For the comparison the NA49 $\Xi^0(1530)$ peak contains about 150 events [27].

Signal	$\Xi^0(1530)$	$\overline{\Xi^0}(1530)$
Position of the signal [MeV]	1533.0±2.8	1540.0±3.0
Gaussian width σ [MeV]	19.9±3.6	20.7±3.5
Number of events (S)	258	200
S/B ratio	0.59	0.75

Table 8.5: Characteristics of the $\Xi^0(1530)$ and $\overline{\Xi^0}(1530)$ signals; the PDG values of their masses and FWHM are (1531.80 ± 0.32) MeV and (9.1 ± 0.5) MeV respectively.

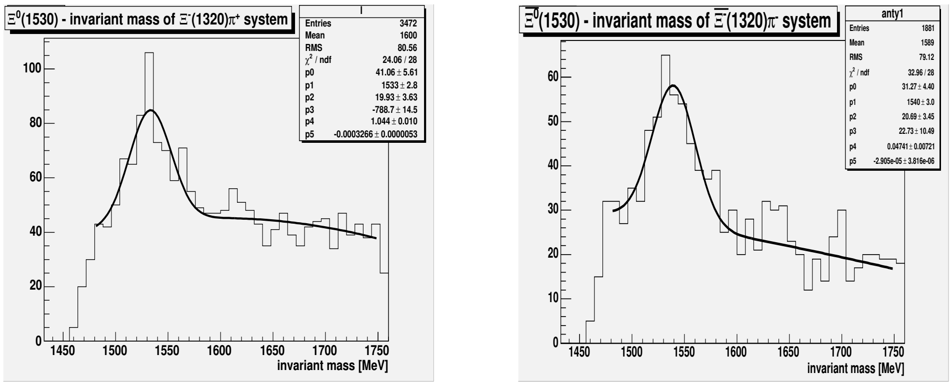

Figure 8.6: $\Xi^0(1530)$ (left) and $\overline{\Xi^0}(1530)$ (right) signals.

Number of events in the peaks are calculated in ± 40 MeV mass windows centred at each peak. Fits are very sensitive to the background shape. Even a small change in the fit range or in the number of events in the background can induce a nonnegligible modifications in the number of the events in the peak. The number of events calculated with different fits can vary by $\pm 15\%$ from the number obtained above.

8.2.2 Comparison of $\Xi^0(1530)$ yields in the Monte Carlo and in the 2002 data

To estimate the cross section for the $\Xi^0(1530)$ hyperon production in the COMPASS experiment, a comparison with a Monte Carlo sample is performed. MC sample was prepared with the PYTHIA 6.2 generator. Generated events were then passed through COMGEANT and reconstructed with CORAL. The $y > 0.07$ cut was imposed at the generation level. The same cut is imposed on the Real Data (RD) sample and results in 270 ± 40 $\Xi^0(1530)$ candidates (the error corresponds to 15% uncertainty mentioned in Sec. 8.2.1 above). The MC sample contains 100 000 generated events, each of them with at least one $\Xi^0(1530)$ particle at the primary vertex. The physical multiplicity of $\Xi^0(1530)$ in the MC sample is 0.00082 (*i.e.* 0.00082 hyperons are produced in each $\mu - N$ interaction) and the trigger efficiency is equal to 0.39. The cross section for the $\mu - N$ interaction is $0.002245 \cdot 10^{-27}\text{cm}^2$. Thus the MC luminosity is:

$$\mathcal{L}_{MC} = \frac{100000}{0.00082 \cdot 0.39 \cdot 0.002245 \cdot 10^{-27}\text{cm}^2} = 139.29 \cdot 10^{36}\text{cm}^{-2} \qquad (8.3)$$

Integrated muon flux for all analysed runs and calculated with the built-in

PHAST 6.008 'spill-time range' function is equal to $276.27{\cdot}10^{11}$. Another method – 'event-event time' – gives a value of $271.55{\cdot}10^{11}$. The difference between both values (1.7%) in comparison with other uncertainties appearing in the analysis is negligible. The Real Data luminosity is the product of a flux and a surface density of the target centres (see Sec. 6.1.2). It is equal to $\mathcal{L}_{RD} = 96.365 \cdot 10^{37}\text{cm}^{-2}$. Selection of $\Xi^0(1530)$ particles in the case of the MC sample is done in the same way as in the case of RD analysis and results in 140 ± 21 $\Xi^0(1530)$ particles. The expected number of $\Xi^0(1530)$ is:

$$N_{expected} = N_{MC}\frac{\mathcal{L}_{RD}}{\mathcal{L}_{MC}} = \frac{140 \cdot 96.36 \cdot 10^{37}\text{cm}^{-2}}{139.29 \cdot 10^{36}\text{cm}^{-2}} = 969 \pm 145 \tag{8.4}$$

The ratio of the expected (MC simulation) yield of $\Xi^0(1530)$ candidates to the measured one is:

$$\left(\frac{N_{expected}}{N_{RD}}\right)_{\Xi^0(1530)} = \left(\frac{969}{270}\right) = 3.59 \pm 0.76 \tag{8.5}$$

The obtained value is consistent with those for K^0 and Λ^0 equal 3.13 and 3.60 respectively (see Sec. 6). The errors on those two numbers were not calculated but they seem to be smaller than an error on the 3.59 value.

8.2.3 Cross section for the $\Xi^0(1530)$ production in COMPASS

The $\Xi^0(1530)$ production cross section is defined as the ratio of the total number of produced $\Xi^0(1530)$ particles and the integrated luminosity in RD:

$$\sigma_{\Xi(1530)} = \frac{N_{\Xi(1530)}}{\mathcal{L}_{RD}} \tag{8.6}$$

The total number of produced particles is equal:

$$N_{\Xi(1530)} = 270 \cdot 3.59 \cdot \frac{100000}{140} = 692000 \pm 207000 \tag{8.7}$$

The 100 000/140 factor corresponds to the geometrical acceptance of the detector and to the efficiency of the reconstruction – the number of reconstructed $\Xi^0(1530)$ particles in the Monte Carlo is 140 while 100 000 is the total number of generated events containing at least one $\Xi^0(1530)$ decaying in the considered channel.

Cross section for the $\Xi^0(1530)$ production measured in COMPASS in the muon-nucleon interactions at the muon beam energy of 160 GeV is equal to:

$$\sigma_{\Xi(1530)} = \frac{N_{\Xi(1530)}}{\mathcal{L}_{RD}} = \frac{692000}{96.36 \cdot 10^{37}\mathrm{cm}^{-2}} = (0.72 \pm 0.22)\mathrm{nb} \tag{8.8}$$

It should be stressed that the errors on $N_{\Xi(1530)}$ and $\sigma_{\Xi(1530)}$ result only from 15% inaccuracy in the estimate of the number of $\Xi(1530)$ hyperons in the MC and RD samples.

Chapter 9

Analysis of the $\Xi_{3/2}$ pentaquark states

Four ($\Xi^{--}_{3/2}$, $\Xi^{0}_{3/2}$, $\overline{\Xi^{--}_{3/2}}$, $\overline{\Xi^{0}_{3/2}}$) "NA49 pentaquark" states [13] can be studied in the COMPASS spectrometer. They should be visible in $\Xi^-\pi^-$, $\Xi^-\pi^+$, $\overline{\Xi^-}\pi^+$, $\overline{\Xi^-}\pi^-$ invariant mass spectra, respectively. To obtain these spectra cuts identical to those from Sec. 8.2.1 are used. All four mass distributions are added together to enhance the significance of a possible peak. Neither the individual mass spectra (Fig. 9.1) nor the combined one (Fig. 9.2) demonstrate any significant signals around 1862 MeV.

An exponential function is fitted to the combined spectra in the range 1600–2600 MeV. The function seems to be a very good approximation of the background. Knowing the parameters of the fitted curve the number of background events (B) in a given mass range can be calculated. If a pentaquark peak was present and contained S events, its significance would be $S/\sqrt{S+B}$ where B is calculated in the mass range where the peak appeared. Knowing B in different parts of the spectrum, it is possible to estimate the number of required signal events to obtain a peak centered at a given mass and having a given width and significance greater than $3\,\sigma$. Four different widths of a peak were considered – 18, 30, 42 and 60 MeV (this corresponds to 3, 5, 7 and 10 bins in Fig. 9.2). The peak observed by the NA49 collaboration [13] has a width of 17 MeV and the prediction made in [3] suggests the $\Xi_{3/2}$ pentaquark width about 40 MeV. The required number of events can be translated into the total cross section for the $\Xi^{--}_{3/2}$, $\Xi^{0}_{3/2}$, $\overline{\Xi^{--}_{3/2}}$, $\overline{\Xi^{0}_{3/2}}$ pentaquarks production. The number of particles expected in the $3\,\sigma$ peak have to be multiplied by the factor of $3.59 \cdot 100000/140$ (see Sec. 8.2.3) and then divided by the $\mathcal{L}_{RD}$ value. First of these steps is based on two general assumptions:

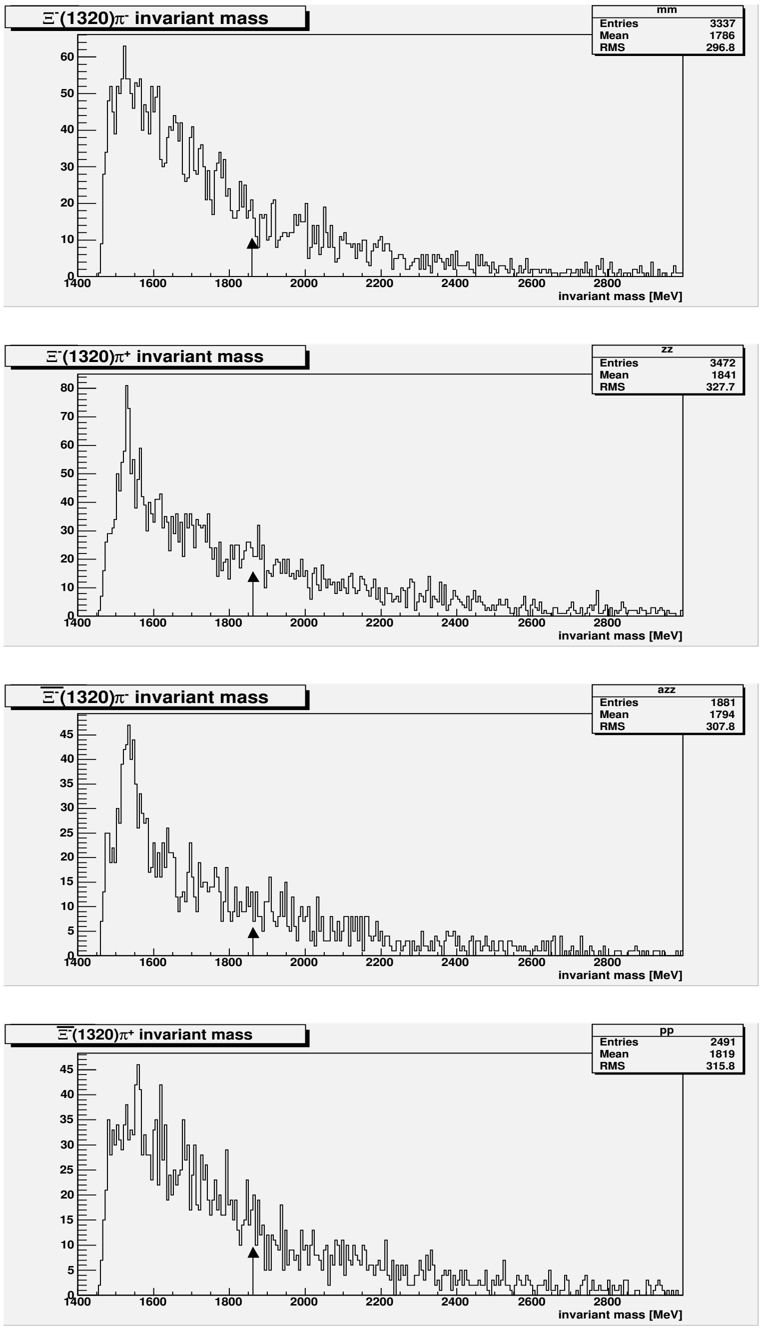

Figure 9.1: $\Xi^-\pi^-$, $\Xi^-\pi^+$, $\overline{\Xi^-}\pi^-$ and $\overline{\Xi^-}\pi^+$ invariant mass distributions. An arrow indicates the 1862 MeV value.

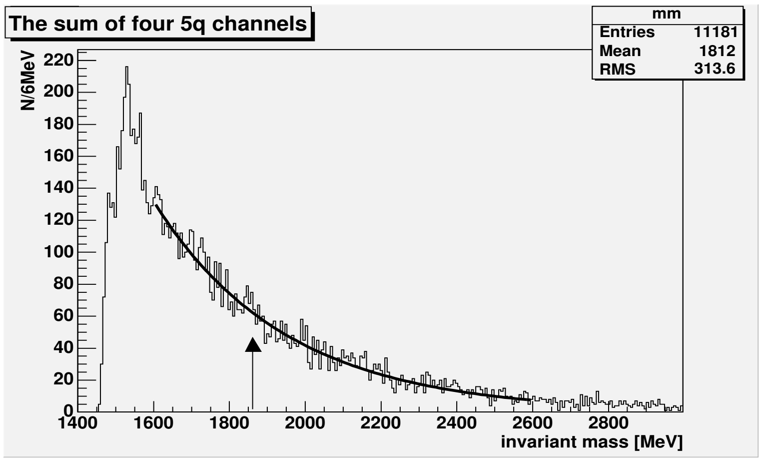

Figure 9.2: Combined plot of $\Xi^-\pi^-$, $\Xi^-\pi^+$, $\overline{\Xi^-}\pi^-$ and $\overline{\Xi^-}\pi^+$ invariant mass distributions. An arrow indicates the 1862 MeV value.

- The spectrometer acceptance in the investigated mass range (1600–2600 MeV) does not depend on the mass of the decaying particle, and is equal to the acceptance for the $\Xi^0(1530)$ particle.

- The spectrometer acceptance does not depend on the sign of the hyperon decay products, *i.e.* the acceptance is the same for $\Xi^-\pi^-$, $\Xi^-\pi^+$, $\overline{\Xi^-}\pi^-$ and $\overline{\Xi^-}\pi^+$.

The obtained cross sections are presented in Fig. 9.3. Since no signal is observed, the values on the plot are the estimates of the upper limits of the cross sections for the summed $\Xi^{--}_{3/2}$, $\Xi^0_{3/2}$, $\overline{\Xi^{--}_{3/2}}$, $\overline{\Xi^0_{3/2}}$ pentaquarks production. In particular cross section limits for pentaquarks of mass 1862 MeV can be read off the plots in Fig. 9.3. These cross sections are: 0.12 ±0.03, 0.15±0.04, 0.18±0.05, and 0.21±0.05 nb for the 18, 30, 42, 60 MeV signal widths, respectively. Uncertainties are calculated including only errors mentioned at the end of Sec. 8.2.1.

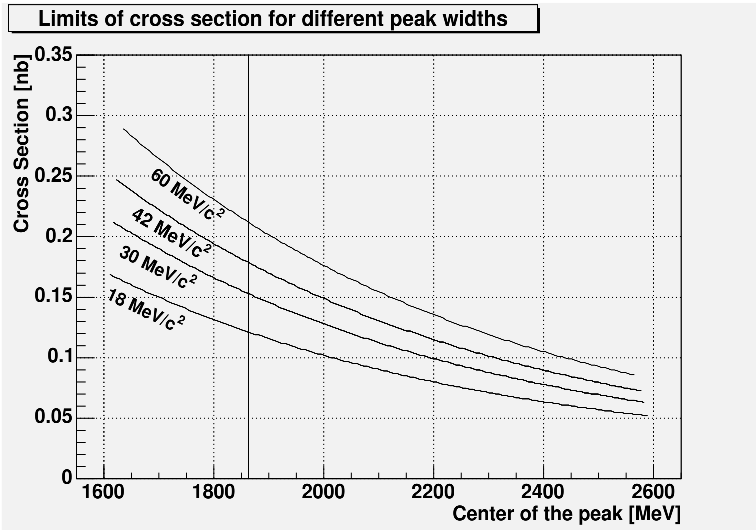

Figure 9.3: Upper limits for cross section for the summed $\Xi_{3/2}^{--}$, $\Xi_{3/2}^{0}$, $\overline{\Xi_{3/2}^{--}}$, $\overline{\Xi_{3/2}^{0}}$ pentaquark production. Each line corresponds to a given width: 18, 30, 42, 60 MeV of a 3 σ hypothetical signal. A vertical black line indicates 1862 MeV.

Chapter 10

Summary and outlook

Several experiments have recently announced an observation of pentaquark states. The existence of such states is not forbidden by the quark model. The search for pentaquarks was also performed on the data from μN interactions taken by COMPASS experiment.

The analysis was performed on the 2002 COMPASS data. The K^0, Λ^0, $\overline{\Lambda^0}$, Ξ^- and $\overline{\Xi^-}$ states were reconstructed. The reconstruction was optimized to obtain a high signal-to-background ratio and a high statistics. A summary of the collected K^0, Λ^0, $\overline{\Lambda^0}$, Ξ^- and $\overline{\Xi^-}$ samples is presented in Table 10.1.

Particle	Number of events	Signal-to-background ratio
K^0	1 804 620	9.42
Λ^0	339 206	1.45
$\overline{\Lambda^0}$	193 340	0.96
Ξ^-	3126	2.51
$\overline{\Xi^-}$	1883	2.27

Table 10.1: Summary of K^0, Λ^0, $\overline{\Lambda^0}$, Ξ^- and $\overline{\Xi^-}$ signals.

It was found that the ratios of the K^0 and Λ^0 yields in the data and in the Monte Carlo are 3.13 and 3.60 respectively, a discrepancy not yet fully understood by the Collaboration.

Search for the $\Theta^+ \to pK^0 \to p\pi^+\pi^-$ and $\Xi_{3/2} \to \Xi\pi \to \Lambda^0\pi\pi \to p\pi\pi\pi$ pentaquarks and for the respective antipentaquarks was performed. No signals of Θ^+ were obtained, not even with the RICH identification of (high energy) particles. However studies of the Θ^+ are highly affected by a lack of identification of low energy protons. In the case of the $\Xi_{3/2}$ pentaquark it was shown that the statistics and resolution of the 2002 COMPASS data are comparable to the NA49 results. No peaks in any of the four possible decay channels of $\Xi_{3/2}$ pentaquarks was observed in the data. Upper limits of the cross section for the summed $\Xi^{--}_{3/2}$, $\overline{\Xi^{--}}_{3/2}$, $\Xi^{0}_{3/2}$ and $\overline{\Xi^{0}}_{3/2}$ production in COMPASS were estimated. For the $\Xi_{3/2}$ pentaquarks of a mass and width observed in NA49 this limit is equal to about 0.12 nb. A similar analysis including the 2003 data is planned.

All the results presented in this thesis are preliminary. Many aspects of the COMPASS detector performance and the reconstruction efficiency are not yet fully understood. Studies of these problems are in progress.

Acknowledgements

I would like to express my gratitude to the following people for their help, support and assistance in preparing this thesis:

- Barbara Badełek for her supervision, enthusiasm, patience, fruitful discussions and a great excursion to Chamonix.
- The entire Polish COMPASS group for their helpful advices and comments.
- Other people with whom I was working, especially Horst Fisher, Jörg Pretz, Yann Bedfer, Jean-Marc Le Goff, Vadim Alexakhin, Alexandre Korzenev and Sergei Gerassimov.
- Gabriela Głębocka for supporting me through my studies and making my work and life worthwhile.
- And anybody I missed who deserves a mention.

Thank you!

Bibliography

[1] The Review of Particle Physics, Phys. Lett. **B170**, 289 (1986).

[2] M. Praszałowicz, in *Skyrmions and Anomalies*, Proceedings of the Cracow Workshop on Skyrmions and Anomalies, Mogilany, Poland, eds M. Jeżabek and M. Praszałowicz, World Scientific (1987) p.112.

[3] D. Diakonov, V. Petrov and M.V. Polyakov, Z. Phys. **A359** (1997) 305.

[4] SPring-8; T. Nakano *et al.*, Phys. Rev. Lett. **91**, 012002 (2003).

[5] CLAS; S. Stepanyan *et al.*, Phys. Rev. Lett. **91**, 252001 (2003).

[6] CLAS; V. Kubarovsky *et al.*, Phys. Rev. Lett. **92**, 032001 (2004).

[7] DIANA; V.V. Barmin *et al.*, Phys. Atom. Nucl. **66**, 1715 (2003).

[8] SAPHIR; J. Barth *et al.*, hep-ex/0307083.

[9] HERMES; A. Airapetian *et al.*, hep-ex/0312044.

[10] ZEUS; S. Chekanov *et al.*, hep-ex/0403051.

[11] SVD-2; A. Aleev *et al.*, hep-ex/0401024.

[12] WA21, WA25, WA59, E180, E632; A.E. Asratyan, A.G. Dolgolenko and M.A. Kubantsev, hep-ex/0309042.

[13] NA49; C. Alt *et al.*, Phys. Rev. Lett. **92**, 042003 (2004).

[14] H1; A. Aktas *et al.*, hep-ex/0403017.

[15] R.L. Jaffe and F. Wilczek, Phys. Rev. Lett. **91**, 232003 (2003).

[16] H.G. Fisher and S. Wenig, hep-ex/0401014.

[17] J. Podolanski, R. Armenteros, Philosophical Magazine **45**, 13 (1954).

[18] The ROOT System Home Page, http://root.cern.ch.

[19] K. Hagiwara *et al.*, The Review of Particles Physics, Phys. Rev. **D66**, 010001 (2002).

[20] Y. Bedfer (COMPASS), private communication, July 2003.

[21] O.A. Grajek, A. Korzenev and A. Sandacz, *Exclusive* ρ^0 *and* ϕ *production from COMPASS 2002 data*, COMPASS note 2002-15.

[22] K. Schoenning, diploma thesis, *Study of the COMPASS spectrometer performance using* K_s^0 *events*, Uppsala University, 2003, http://wwwcompass.cern.ch/compass/publications.

[23] V. Alexakhin, A. Kotzinian, M. Sapozhnikov, N. Vlasov, *Results on* Λ^0 *and* $\overline{\Lambda^0}$ *production from data on P2D period of run 2002*, COMPASS note 2003-1.

[24] T. Sjöstrand, private communication, May 2003.

[25] J.M. Le Goff, A. Magnon, G. Mallot, J. Pretz, *Global performances for the open charm channel*, COMPASS note 2004-2.

[26] V. Alexakhin (COMPASS), private communication, August 2003.

[27] H.G. Fischer (NA49), private communication, September 2003.